5-2023

First-Principal Investigations of the Electronic, Magnetic, and Thermoelectric Properties of CrTiRhAl Quaternary Heusler Alloy

Shuruq Alsayegh
University of Arkansas-Fayetteville

First-Principal Investigations of the Electronic, Magnetic, and Thermoelectric Properties of CrTiRhAl Quaternary Heusler Alloy

A thesis submitted in partial fulfillment
of the requirements for the degree of
Master of Science in Microelectronics-Photonics

by

Shuruq Alsayegh
Princess Norah Bint Abdulrahman University
Bachelor of Physics, 2012

May 2023
University of Arkansas

This thesis is approved for recommendation to the Graduate Council

Bothina H. Manasreh, Ph.D.
Thesis Director

Omar Manasreh, Ph.D.
Committee Member

Hugh Churchill, Ph.D.
Committee Member

Matt Leftwich, Ph.D.
Ex-Officio Member

The following signatories attest that all software used in this thesis was legally licensed for use by Shuruq Alsayegh for research purposes and publication.

Ms. Shuruq Alsayegh, Student	Dr. Bothina H. Manasreh, Thesis Director

This dissertation was submitted to http://www.turnitin.com for plagiarism review by the TurnItIn company's software. The signatories have examined the report on this dissertation that was returned by TurnItIn and attest that, in their opinion, the items highlighted by the software are incidental to common usage and are not plagiarized material.

Dr. Matt Leftwich, Program Director	Dr. Bothina H. Manasreh, Thesis Director

Abstract

Density functional theory calculations are performed to investigate the electrical electronic, magnetic, and thermoelectric properties of CrTiRhAl quaternary Heusler alloy (QHA). The type-I atomic configuration is found to be the most stable structure of this alloy. The CrTiRhAl QHA exhibits a half-metallic ferromagnetic structure with a narrow band gap at one spin channel (semiconductor), and a metallic behavior at the other spin channel. This corresponds to a 100% spin-polarization, making it ideal for potential spintronic applications. Applying the semi-classical Boltzmann theory, the Seebeck coefficient, electrical conductivity, and electronic thermal conductivity of CrTiRhAl alloy were calculated. The predicted figure of merit (*ZT*) was found to be low (0.4 at 300K), which is not promising for thermoelectric applications.

Keywords: Quaternary Heusler alloy, magnetic properties, lattice thermal conductivity, thermoelectric properties.

Acknowledgments

First and foremost, I want to thank God Almighty for giving me the opportunity and direction that have helped me achieve my objective and succeed on this segment of my life's journey.

Dr. Bothina H. Manasreh has been my thesis chair and has been very helpful and encouraging throughout my time in graduate school and with this research project. This thesis would not have been feasible without her perceptive comments, guidance, and support throughout the years.

Drs. Omar Manasreh and Hugh Churchill, who served as members of my committee, have my sincere appreciation. I'd also want to thank Renee Jones Hearon, Dr. Wise, and Dr. Matthew for their unwavering and invaluable aid during this process. My warmest appreciation would also go to my friends and colleagues in the research group.

Lastly, I would want to express my deepest appreciation to my sponsors the Saudi Arabian Cultural Mission, for making it possible for me to further my studies and learn new things. In addition, I'd want to express my appreciation to the University of Arkansas's high-performance computer center for helping us with our computations.

Dedication

I dedicate this thesis to my husband Mohammed and my little boys Yousef and Ammar, who have been a continuous source of support and encouragement during the struggles of graduate school. I'm grateful beyond words to have you in my life. This work is also dedicated to my parents, Abdullah and Badryah, who have always loved me unconditionally and whose strong character has inspired me to put in a lot of effort to get what I want.

My sisters and best friends Norah, Manar, and Fajer, and lovely brothers Naif and Ahmed who believed and supported me every day during this journey are honored by the dedication of my thesis.

Table of Contents

List of Figures

List of Tables

List of Published Papers

Chapter 4 was published/accepted in scientific journal that is listed below with minor modifications.

Chapter 4 : Alsayegh S, Alqurashi H, Andharih E, Hamad B, Manasreh MO. First-principal investigations of the electronic, magnetic, and thermoelectric properties of CrTiRhAl quaternary Heusler alloy. Journal of Magnetism and Magnetic Materials 2023;568:170421.

Chapter one: Introduction

Motivation

Scientists have been inspired to look for alternative energy sources by the exponential rise in the demand for existing ones because of the technological revolution. Using fossil fuels has consequences for the environment since the gases produced by their burning contribute to pollution and global warming. The fact that mechanical power only employs 25% of the energy available is a contributing factor to the waste heat issue [1]. To solve the energy dilemma, researchers are developing thermoelectric and geothermal power plants. Thermoelectric technology, which is based on solid-state processes, has gained a lot of attention because of its potential use in power production through waste heat recovery and cooling [2].

Waste heat collection and recycling are two components of an integrated strategy to waste heat management that may dramatically reduce carbon emissions in addition to reducing waste heat generation at the source. Utilizing solid-state energy converters, such as thermoelectric generators TEGs, is one way to facilitate waste heat collection and conversion into usable energy forms like electricity. Because of their ease of use, thermoelectric generators may be used in a wide range of uses, mainly those that produce waste heat at hi temperatures of several hundred degrees. Even so, thermoelectric generators may be employed in a wide variety of settings, from low temperatures such as in human body heat harvesting to high temperatures such as in cement factories, concentrated solar heat exchangers, or NASA exploration rovers [3].

The thermoelectric devices are composed of two distinct kinds of semiconductors (n-type and p-type) that are connected electrically in series and thermally in parallel. In thermoelectric generators, a temperature gradient is used to move carriers from the hot side to the cold side.

This creates a drop in voltage and a flow of current. This is called the Seebeck effect, as shown in Figure 1 (a). In thermoelectric coolers, when a voltage drop is applied to the thermoelectric device, a current flow from one end to the other, carrying heat. This is called the Peltier effect. See Figure 1. (b). [4].

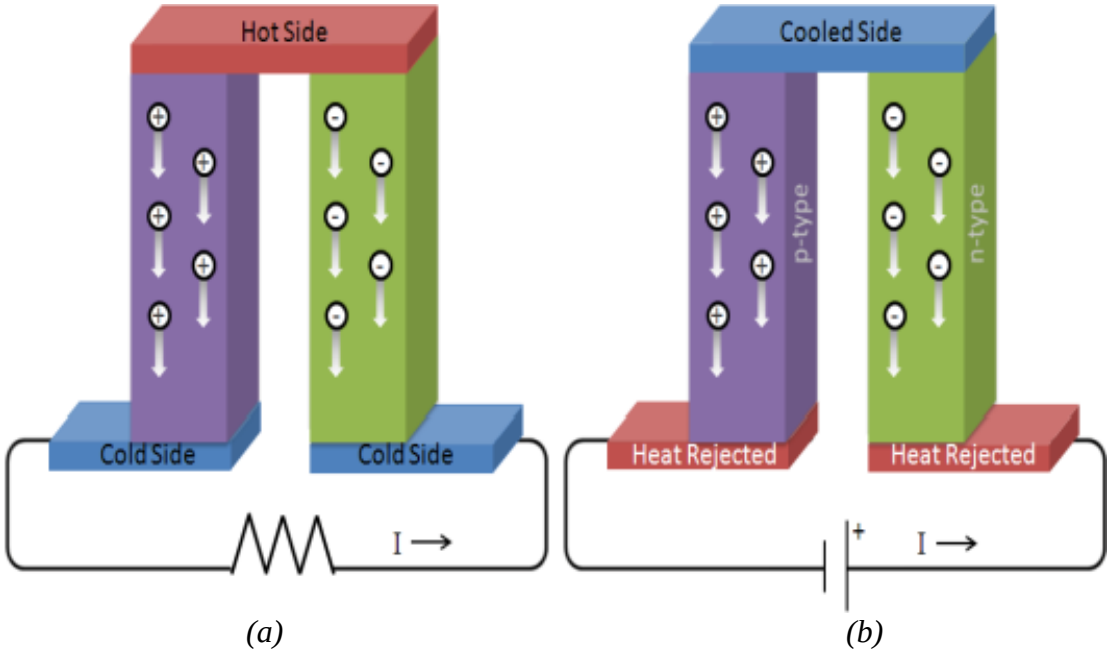

Figure 1: (a) Seebeck effect thermocouple. (b) Peltier effect thermocouple.

The thermoelectric generator (TEG) has several uses beyond only turning waste heat into power [5]. One of these applications is used in space missions such as utilizing TEG for in NASA's spacecraft as a radioisotope usage in outer space [6]. There are many materials that are promising for TEG applications such as Heusler alloys, chalcogenides, and dichalcogenide compounds. Heusler alloys have many interesting properties, such as half metallicity, ferromagnetism, semi-conductivity, spin gapless semi-conductivity, shape memory effect, and superconductivity[7-11].

The outline of this thesis is as follows:

- Chapter 2 presents a literature review of different types Heusler alloys.
- Chapter 3 discusses the Density functional theory and the Boltzmann transport theory.

- Chapter 4 presents the results and discussion of of *CrTiRhAl* quaternary Heusler compound.
- Chapter 6 presents the main concluding remarks.

2. Chapter Two: Background

2.1 Heusler compounds

Heusler alloys have lately sparked considerable attention as prospective possibilities for spintronics and thermoelectric applications. Heusler are classified into four categories: full Heusler alloys (FHA), half-Heusler alloys (HHA), quaternary Heusler alloys (QHAs), and inverse Heusler alloys, look to table (1) [12].

Heusler alloys have a close-packed cubic structure with a four-atom base that forms a face-centered cubic lattice. By choosing different composite elements, Heusler alloys provide a large family of members for cutting-edge research on spintronics and magnetic materials and devices[13].

Heusler compound type	**Chemical Structure Formula**	**Example**
1. Full Heusler compound	X_2YZ	Co_2MnTi
2. Inverse Heusler compound	X_2YZ	Hg_2TiCu
3-Half Heusler compound	XYZ	TiRhAl
4-Quaternary Heusler compound	X$\grave{X}YZ$	CrTiRhAl

Table 1: The different structures of the Heusler compounds

1. Full Heusler compound: The valence electrons of the Y transition-metal atom are less than the valence electrons of the X transition-metal atom.

2. Inverse Heusler compound: The valence electrons of the X atom are less than the valence electrons of Y atom.
3. Half Heusler compound: One of the four sublattices is vacant.
4. Quaternary Heusler compound: The quaternary Heusler compound with the chemical formula X X`YZ is formed by replacing one of the X transition metal atoms by another (X`) in the full Heusler compound, where Y atom has less valence electrons than X` and the latter has less valence electrons than X[13, 14].

The electronic structure of Heusler compounds is very sensitive to pressure changes. A small change in the lattice constant can change a half-metallic structure into a metallic structure or make a nearly half-metallic structure more half-metallic due to the shift of the Fermi level to the middle of the gap[15]. The electronic and magnetic properties of a crystal depend on how its atoms are arranged. If the atoms are in different orders in the same compound, the electronic and magnetic properties are different[16].

In Figure 2, we see schematics of the density of states for different Heusler compounds. Unlike metals and semiconductors, the band structure of certain Heusler compounds is unique, with one spin channel behaving like a metal and the other like a semiconductor[15, 17, 18].
This is referred to as ferromagnetic behavior in the half-metallic state (HMF). There is a possibility that these compounds are spin gapless semiconductors, where the band gap across the Fermi level is zero in both spin channels (E_f)[19]. This means Heusler compounds are ideal candidates for spintronic devices due to their half metallicity and spin gapless features[20].

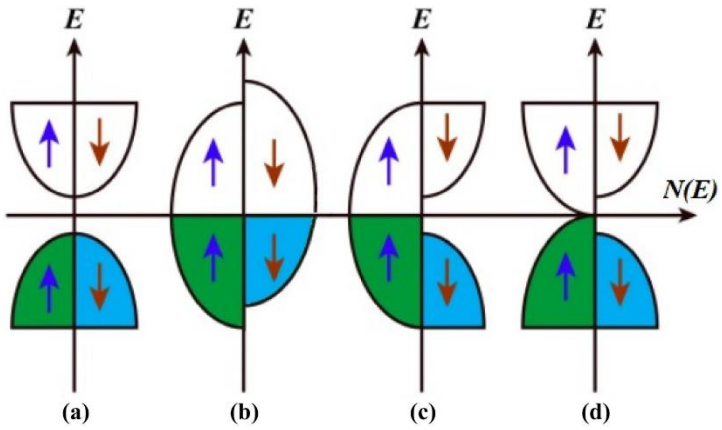

Figure 2: Schematics of the density of states for (a) metallic, (b) semiconductor, (c) HMF, and (d) spin gapless semiconductor[21].

In semiconductors, there is a difference in energy between the top of the valence band and the bottom of the conduction band. At absolute zero, semiconducting materials do not contain any conduction electrons; these electrons do not begin to exist until the material is heated above 0 K.

The high spin polarization is caused by half-metallic ferromagnetism. Spin polarization at Fermi energy may be used to realize electronic characteristics. Spin polarization (P) is written as follows [22].

$$P = \frac{p_{up}(E_F) - p_{dn}(E_F)}{p_{up}(E_F) + p_{dn}(E_F)} \times 100 \qquad \text{(Equation 1)}$$

Where: $p_{up}(E_F)$ spin up density of states at the fermi level E_F, and $p_{dn}(E_F)$ spin dn density of states at the fermi level E_F. Materials with P = 100% possess full half-metallicity, with a zero density of states in either the spin up or spin down channels. The Slater-Pauling rule is a mathematical expression of the relationship between the number of valence electrons and the total spin magnetic moment. The rule is widely known to apply to Heusler compounds [9, 23]. It is utilized for estimating the material's total spin magnetic moment as follow:

$$M_{\text{tot}} = N_{\uparrow} - N_{\downarrow} = (Z_{\text{tot}} - N_{\downarrow}) - N_{\downarrow} = Z_{\text{tot}} - 2N_{\downarrow} \quad \text{(Eqution 2)}$$

Where, M_{tot} , Z_{tot}, $N_{\downarrow}$, and $N_{\uparrow}$ are the total magnetic moment, number of the total valence electrons, spin-down valence electrons and spin-down valence electrons respectively.

The thermoelectric performance of a material can be quantified using the dimensionless figure-of-merit:

$$ZT = \frac{S^2\sigma}{\kappa_e + \kappa_l} \quad \text{(Equation 3)}$$

Where S, σ, κ_e and κ_l are the Seebeck coefficient, electrical conductivity, lattice and electronic and thermal conductivities respectively [24, 25]. A high ZT value indicates that the thermoelectric material has a high conversion efficiency. As shown in Eq 3, there is no upper limit to the value of the ZT.

A higher ZT value can be utilized by increasing the Seebeck coefficient or the electrical conductivity or by lowering the lattice thermal conductivity. Nonetheless when the electrical conductivity goes up, the electronic thermal conductivity also goes up. As a result, the best thermoelectric materials have a ZT ≈ 1. It is well understood that the thermoelectric properties are affected by the electronic structure. According to the following equation, a decrease in the effective mass or a decrease in the carrier concentration causes an increase in the Seebeck coefficient of the material:

$$= \frac{8\pi^2 k_B^2 T}{3eh^2}\, m^3 \left(\frac{\pi}{3n}\right)^{3/2} \quad \text{(Equation 4)}$$

Where, $\kappa_{B,}$ e , h , m, and n are the Boltzmann constant, electronic charge, Planck's constant, effective mass, and carrier concentration, respectively.

Furthermore, according to the following relationship, high mobility (μ) and a small band gap increase electrical conductivity [26].

$$\sigma = ne\mu \quad \text{(Equation 5)}$$

Where, $n, e,\ and\ \mu$ are carrier concentration, electronic charge, and high mobility respectively. The Seebeck coefficient of the materials is an essential feature that may be described as the ratio of the voltage produced to a 1 K temperature differential (V/K). The Seebeck coefficient of metals is found to be quite low, with most metals exhibiting less than μV K^{-1}[27]. Furthermore, at whatever temperature, the electrical to thermal conductivity ratio remains constant. these two features result in low ZT values in metals. Semiconductors, on the other hand, have greater power factor values than metals , making them preferable for thermoelectric materials [28, 29]In recent years, quaternary Heusler compounds have garnered a growing amount of research interest. Some of these compounds have shown features that are encouraging for the development of spintronic devices and thermoelectric applications [9, 30, 31].

2.2 Literature review

Most of the theoretical research of full- and half-Heusler compounds was focused on the electronic, magnetic, and transport features of these compounds. Full-Heusler compounds were the structures that received the most amount of attention among the different kinds of Heusler compounds. Full-Heusler compounds based on cobalt have garnered a lot of interest recently owing to the half-metallic nature and high Curie temperatures of these compounds [32].Gapless semiconductors, or semiconductors with a vanishing gap width, are a subset of this larger category. Because the carrier mobility in these materials is so much higher than in typical semiconductors, they are of particular interest, see figure (3) [33].

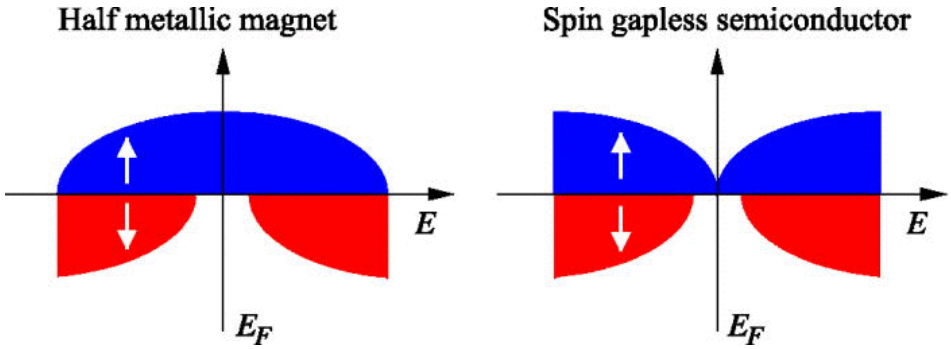

Figure 3: Schematic representation of the density of states of a half-metallic system (left panel) and of a spin gapless semiconductor (right panel). With blue (red) we show the spin-up (spin-down) states[33].

A previous on FeCrRuAl alloy, the spin-polarized density of states (DOS) calculation shows an uncommon spin-gapless half-metallic (SG-HM) behavior, with the majority spin-up channel being metallic and the minority spin-down channel being spin-gapless [34]. Also in another study, Skaftouros. et al, approved that HgCdTe, HgCdSe ,and HgZnSe, have shown a spin gapless semiconducting behavior[33]. Therefore, Heusler alloys can be half-metallic, which means that the band structure of one spin channel acts like a metal and the structure of the other spin channel acts like a semiconductor.

In physics, Curie temperature (T_C) or Curie point is the temperature above which some materials lose their permanent magnetic properties [35]. Previous studies have shown that Heusler alloys, such as TiVFeAl, TiVFeSi, and TiVFeGe exhibit high Curie temperatures [36],[37]. Furthermore, ab initio electronic structure computations for CoFeMnZ (Z = Al, Ga, Si, or Ge) compounds with high Curie temperatures revealed a half-metallic ferromagnetic [16]. Guo et al. studied ZrFeVZ (Z = Al, Ga, In) and they found the QHAs exhibit high Curie temperatures and half-metallic behavior [37].

Using waste heat energy, thermoelectric phenomena provide a potential solution recycle the waste hate to a power for heating and cooling. Heusler compounds have received much

attention due to their potential qualities as excellent thermoelectric materials that may be used for energy harvesting and refrigeration [38-40]. Research on the Heusler alloys RhTiBi, RhTiP, RhTiAs, and RhTiSb discovered that all four have low thermal conductivities and sufficiently high values of power factor, making them good candidates for use in thermoelectric applications [41].

Magnetoelastic couplings, shape memory, magnetic super elasticity, magnetocaloric effects, and barcaloric effects are only some of the numerous useful features shown by Heusler alloys[42, 43]. Those interesting features make the Heusler alloys a very rich field to study and investigate.

3. Chapter Three: Method of calculations

3.1 Schrödinger equation

Here is a general form for the time-dependent Schrödinger equation that describes a many-body system:

$$i\hbar \frac{\partial \Phi(\mathrm{r,R,t})}{\partial \mathrm{t}} = -\frac{\hbar^2}{2\mu}\nabla^2\Phi(\mathrm{r,R,t}) + \mathrm{V}\Phi(\mathrm{r,R,t}) \qquad \text{(Equation 6)}$$

Where, $\hbar$, $\Phi(\mathrm{r,R,t})$, μ, V, are the reduced Planck constant, wavefunction of the ions and electrons, reduced mass, potential, r and R are electron and nuclei coordinates. In this research, the energy was independent of time. Therefore, separation of variables was used to write $\Phi(\mathrm{r,R,t})$ as follow:

$$\Phi(r,R,t) = \Phi(r,R)\varphi(t) \qquad \text{(Equation 7)}$$

As a result, we can write down the time-independent Schrödinger equation as:

$$\hat{\mathrm{H}}\Phi(r,R) = E\Phi(r,R) \qquad \text{(Equation 8)}$$

$$\hat{\mathrm{H}} = \hat{\mathrm{T}}_\mathrm{e} + \hat{\mathrm{T}}_\mathrm{N} + \hat{\mathrm{V}}_\mathrm{ee} + \hat{\mathrm{V}}_\mathrm{eN} + \hat{\mathrm{V}}_\mathrm{NN} \qquad \text{(Equation 9)}$$

Here E is the energy and $\hat{\mathrm{H}}$ stands for the Hamiltonian operator. Where $\hat{\mathrm{T}}_\mathrm{e}$ and $\hat{\mathrm{T}}_\mathrm{N}$ are the kinetic energy of an electron and the nuclei, respectively, and $\hat{\mathrm{V}}_\mathrm{ee}$, $\hat{\mathrm{V}}_\mathrm{eN}$ and $\hat{\mathrm{V}}_\mathrm{NN}$, are the potential energy of electron-electron, electron- nucleus, and nucleus-nucleus interactions, respectively. The $\hat{\mathrm{T}}_\mathrm{e}$,$\hat{\mathrm{T}}_\mathrm{N}$, $\hat{\mathrm{V}}_\mathrm{ee}$, $\hat{\mathrm{V}}_\mathrm{eN}$, and $\hat{\mathrm{V}}_\mathrm{NN}$ are given as:

$$\hat{\mathrm{T}}_\mathrm{e} = -\frac{\hbar^2}{2m_2}\sum_{i=1}^{N_e}\nabla_i^2 \qquad \text{(Equation 10)}$$

$$\hat{\mathrm{T}}_\mathrm{N} = -\frac{\hbar^2}{2m_2}\sum_{N=1}^{N}\nabla_N^2 \qquad \text{(Equation 11)}$$

$$\hat{\mathrm{V}}_{\mathrm{ee}} = \sum_{i=1}^{N_e} \frac{\mathrm{e}^2}{|r_i - r_j|} \qquad \text{(Equation 12)}$$

$$\hat{\mathrm{V}}_{\mathrm{eN}} = \sum_{i=1}^{N_e} \frac{Z_I \mathrm{e}^2}{|R_I - r_j|} \qquad \text{(Equation 13)}$$

$$\hat{\mathrm{V}}_{\mathrm{NN}} = \sum_{i=1}^{N_e} \frac{Z_I Z_J \mathrm{e}^2}{|R_I - R_J|} \qquad \text{(Equation 14)}$$

Here m_e and M_N are the mass of the electron and the nucleus, respectively, e is the electron charge, and Z is the charge of the nucleus. For many body problems, solving the Schrödinger equation precisely using the Hamiltonian of Equation 9 is extremely difficult. It can, however, only be solved for simple problems such as the hydrogen atom. As a result, some approximations are required to solve this problem.

3.2 Born-Oppenheimer Approximation

Since the mass of a proton is four orders of magnitude more than that of an electron, the Born-Oppenheimer assumption holds that nuclei do not move. The huge mass of nuclei in their denominators makes it difficult to ignore the kinetic energy of nuclei and the potential energy of the nucleus-nucleus interaction if nuclei are believed to be static, which allows the problem to be simplified to the electronic component. Using the Born-Oppenheimer approximation, we can transform the many-body issue into a many-electron problem, and the Hamiltonian may be written as:

$$\widehat{H_e} = \hat{\mathrm{T}}_{\mathrm{e}} + \hat{\mathrm{V}}_{\mathrm{ee}} + \hat{\mathrm{V}}_{\mathrm{eN}} + \hat{\mathrm{V}}_{\mathrm{NN}} \qquad \text{(Equation 15)}$$

Here $\widehat{H_e}$ is the Hamiltonian of the electronic part. Therefore, (E_0) the total energy of ground state can be expressed as $E_0 = \langle \Psi_0 | H_e | \Psi_0 \rangle + V_{NN}$, here Ψ_0 is the wavefunction of the electronic ground state.

For a system with many particles, solving this equation remains challenging because of the presence of many electrons. Therefore, two different approximation methods are used to solve this issue. Hartree-Fock theory and density-functional theory are the first.

3.3 Hartree-Fock Approximation

Hartree suggested in 1928 that the electron is influenced by a potential that is the mean between the potentials of the electrons and the nucleus [44]. To use this potential to solve the Schrödinger equation, Hartree assumed that the wavefunction of a system is a multiplication of the wavefunctions of the individual particles $\phi i(i)$.

$$\Psi(1, \dots, N) = \phi 1(1)\phi 2(2) \dots \phi N(N) \qquad \text{(Equation 16)}$$

Where, $\phi i(i)$ depends on position and spin of electron number (i). Fermions like electrons, have a spin that is half integral. In accordance with the Pauli exclusion principle, the wavefunction of these particles should ensure that no two electrons have the same quantum numbers. However, because electron-electron interactions are not described, the Hartree wavefunction is anti-symmetric. Hartree-Fock employed a single Slater determinant to write the complete wavefunction of numerous particle systems and thus allow the wavefunction to flip signs when two electrons are swapped as follow:

$$\Psi(1, \dots, N) = \frac{1}{\sqrt{N_i}} \begin{vmatrix} \Phi_1(1) & \Phi_1(2) & \cdots & \Phi_1(N) \\ \Phi_2(1) & \Phi_2(2) & \cdots & \Phi_2(N) \\ \vdots & & \ddots & \vdots \\ \Phi_N(1) & \Phi_N(2) & \cdots & \Phi_N(N) \end{vmatrix} \qquad \text{(Equation 17)}$$

where the subscript indicates the eigenstate and the number in the parenthesis represents the electron's atomic number. Now, Equation 17 satisfies the Pauli exclusion principle by showing that switching any two electrons around will flip the sign of the wavefunction. If two electrons are in the same quantum state, the wavefunction collapses to zero. Since the Hartree solution does not account for an exchange term that might minimize the ground state energy and provide the best approximation to the actual energy, the Hartree-Fock wavefunction incorporates this term. The Hartree-Fock wavefunction of one electron ϕi(r) provided as:

$$(-\frac{\hbar^2}{2\mu}\nabla^2 + V_{eff})(\mathrm{r})\phi_i(\mathrm{r}) = \varepsilon_i\phi_i(\mathrm{r}) \qquad \text{(Equation 18)}$$

Here, V_{eff} are the effective potential that's consist of electron-electron (Vee), electron-ion (VeN), and exchange (Vx) potentials respectively.

$$Vee(r) = -\frac{\mathrm{Z}e^2}{|\vec{\mathrm{r}}|} \qquad \text{(Equation 19)}$$

$$V_{eN}(r) = e^2 \sum_{i\neq j} \int \frac{|\,\phi_j(\overrightarrow{\mathrm{r}_2})\,|}{|\overrightarrow{\mathrm{r}_1} - \overrightarrow{\mathrm{r}_2}\,|} d\overrightarrow{\mathrm{r}_2} \qquad \text{(Equation 20)}$$

$$V_{eN}(r) = -e^2 \sum_{j,i\neq j} \int \frac{\phi_j(\overrightarrow{\mathrm{r}_2}) * \phi_i(\overrightarrow{\mathrm{r}_2})}{|\overrightarrow{\mathrm{r}_1} - \overrightarrow{\mathrm{r}_2}\,|} d\overrightarrow{\mathrm{r}_2} \qquad \text{(Equation 21)}$$

Atoms and molecules can benefit from the Hartree-Fock approximation. However, it requires a lot of computing power and produces inaccurate results when dealing with substances that have a lot of electrons.

3.4 Density Functional Theory

In 1927, Thomas and Fermi proposed a way to express the system's total energy (E_{tot}) as a function of the density of individual electrons $\rho(\vec{r})$. This was the first step in reducing the many-body wavefunction to the one-body density form [45].

$$E_{tot}[\rho(\vec{r})] = \frac{3(3\pi^2)^{2/3}}{10}\int \rho(\vec{r})^{\frac{5}{3}} d^3\vec{r} - Z\int \frac{\rho(\vec{r})}{r} d^3\vec{r} + \frac{1}{2}\iint \frac{\rho(\vec{r_1})\rho(\vec{r_2})}{|\vec{r_1}-\vec{r_2}|} d^3\vec{r_1}\, d^3\vec{r_2} \quad \text{(Equation 21)}$$

Here, the density of one electron is normalized to the total number of electrons (N).

$$\int \rho(\vec{r})\ d^3\vec{r} = N \quad \text{(Equation 22)}$$

After some time, Hohenberg and Kohn presented the fundamental formulation of the density functional theory, which posits that the total electronic energy is a functional of the electron density [46]. The system's wavefunction and energy can be calculated from the electron density. Thus, the electron density is solved, which consists of only three spatial variables, rather than the wavefunction, which consists of 3N variables. The functional was initially established by Hohenberg and Kohn as the electron density that minimizes the total electronic energy, which is the solution to the ground state Schrödinger equation [46]. According to Hohenberg and Kohn's theorems, the total energy functional at ground state is:

$$E_{tot}[\rho(\vec{r})] = F_{HK}[\rho(\vec{r})] = \int \rho(\vec{r})\, N_{eN}\vec{r} d\vec{r} \quad \text{(Equation 23)}$$

Where $F_{HK}[\rho(\vec{r})]$ stands for Hohenberg-Kohn functional which is the sum of the exact kinetic and electron-electron potential energy functionals as follow:

$$F_{HK}[\rho(\vec{r})] = T[\rho(\vec{r})] + V[\rho(\vec{r})] = T_0[\rho(\vec{r})] + V_H[\rho(\vec{r})] + V_{xc}[\rho(\vec{r})] \quad \text{(Equation 24)}$$

Where, $T[\rho(\vec{r})]$, $V[\rho(\vec{r})]$, $T_0[\rho(\vec{r})]$, $V_H[\rho(\vec{r})]$ and $V_{xc}[\rho(\vec{r})]$, are the kinetic potential functional, electron-electron potential functional, kinetic of non-interacting particles functional, Hartree

potential energy functional and exchange correlation energy functional respectively; which is defined by the sum of the exchange $Vx[\rho(\vec{r})]$ and the correlation $Vc[\rho(\vec{r})]$ potentials.

Although it is included into the total energy of the Hartree-Fock solution, the exchange potential is not considered in the Hartree solution.

$$V_x = E_{HF} + E_H \quad \text{(Equation 25)}$$

While the Hartree-Fock solution's total energy does not account for the correlation potential, the exact total energy does.

$$V_c = E_{exact} + E_{HF} \quad \text{(Equation 26)}$$

The total energy functional can be expressed as follows:

$$E_{tot}[n(\vec{r})] = T_0[n(\vec{r})] + V_H[n(\vec{r})] + V_{xc}[n(\vec{r})] + V_{En}[n(\vec{r})] \quad \text{(Equation 27)}$$

Since the functional form of the exchange-correlation energy is still a mystery, it is impossible to solve Equation 27. The density of electrons was proposed to be expressed in terms of a collection of wavefunctions by Kohn and Sham , with each wavefunction representing a single electron [47]. This leads us to define the ground electron density as the total number of electrons in all of the occupied Kohn-Sham orbitals (ψ_i).

$$n(\vec{r}) = \sum_{i=0}^{occu} \psi_i^*(\vec{r})\psi_i(\vec{r}) \quad \text{(Equation 28)}$$

Thus, Equation 28 represents a solution to the Kohn-Sham equation for a single electron in its ground state.

$$\left(T + V_{eff}\right)\psi_i = E_i\psi_i \quad \text{(Equation 29)}$$

$$V_{eff} = V_{eN} + V_H + V_{xc} \quad \text{(Equation 30)}$$

$$V_{eN} = \frac{1}{4\pi\varepsilon_0}\sum_{n=1}\frac{Z_n e^2}{|\vec{r_i} - \vec{R_n}|} \quad \text{(Equation 31)}$$

$$V_H = \frac{1}{4\pi\varepsilon_0}\int \frac{n(\vec{r_j})e^2}{|\vec{r_i} - \vec{r_j}|}\, d\vec{r_j} \quad \text{(Equation 32)}$$

$$V_{xc} = \frac{\delta V_{xc}[n(\vec{r})]}{\delta n(\vec{r})} \quad \text{(Equation 33)}$$

Therefore, for the set of atoms [47], the total ground state energy is expressed by:

$$E_{tot}(R_1, \dots, R_n) = \Sigma E_i - \frac{1}{2} E_H[n_0(\vec{r})] + E_{xc}[n_0(\vec{r})] - \int V_{xc}\rho_0 \, d\vec{r} + V_{NN}(R_1, \dots, R_n) \quad \text{(Equation 34)}$$

Using Kohn and Sham equations to calculate ground-state densities, the density functional theory matured into a useful tool. Its application in describing the electronic structure of atoms, molecules, and bulk materials is widespread in the physical and chemical sciences.

3.5 Exchange-correlation energy approximations

Density functional theory relies on an accurately defined exchange-correlation functional in order to determine the energy of the ground state. The local density approximation (LDA) [47] and the generalized gradient approximation (GGA) [48] are the two most used approximations used to estimate the exchange-correlation energy. There are more advanced exchange-correlation functionals such as hybrid functionals where part of Hartree-Fock exchange potential is included in these functionals.

3.5.1 Local density approximation (LDA)

The electron density of a system is approximated here by the density of a homogeneous electron gas, which is held constant as follows:

$$E_{xc}^{LDA} = \int n(\vec{r})\epsilon_{xc}\big(n(\vec{r})\big)d\vec{r} \quad \text{(Equation 35)}$$

The LDA approximation divides $\epsilon_{xc}n(\vec{r})$ into an exchange and correlation term as follows:

$$\epsilon_{xc}n(\vec{r}) = \epsilon_x n(\vec{r}) + \epsilon_c n(\vec{r}) \quad \text{(Equation 36)}$$

Quantum Monte Carlo simulations are used to obtain the correlation term, while the exchange term can be solved analytically [49]. It's important to remember that in practice, electron densities are not constant. As a result, this approximation is only applicable to systems in which the density changes very gradually.

3.5.2 Generalized gradient approximation (GGA)

A new method for the exchange correlation functional incorporates the electron density gradient in addition to the uniform electron density, which improves LDA.

$$E_{xc}^{GGA} = \int n(\vec{r})\epsilon_{xc}\big(n(\vec{r})\big)\mathrm{F}(|\nabla \mathrm{n}(\vec{r})|)\ d\vec{r} \qquad \text{(Equation 37)}$$

Generalized gradient approximation (GGA) is a new approximation that performs well for solids. GGA can be measured in a variety of ways. The two most common are the Perdew-Burke-Ernzerhof (PBE) [48] and the PBE-sol [50].

3.6 Self-consistent solution

The dependence of the Hartree and exchange-correlation potentials on the electron density is demonstrated by the equations 32 and 33. The electron density can be obtained by solving the single-particle wavefunction. However, by solving the Khon-Sham equations, we can obtain these wavefunctions. This issue is addressed via the self-consistent procedure. To determine the wavefunctions of a single particle, one must first solve the Khon-Sham equations based on a best guess of the initial electron density. Based on the results of the single particle wavefunction calculations, a new electron density is established. We can determine the ground state energy if the change in electron density is equivalent to the change in density at the

beginning of the experiment. When the two densities are unequal, the process is restarted with the new initial electron density. For as long as the delta between input and output electron density exceeds the convergence c

criterion, this process is repeated.

3.7 Boltzmann Transport Theory

The Boltzmann transport equation describes the movement of electrons or holes in a system subject to a temperature gradient or external field. The Fermions (electrons) in a static environment follow the $f0(\varepsilon)$ distribution function described by the Fermi-Dirac equation:

$$f_0(\varepsilon) = \frac{1}{1+EXP(\frac{\varepsilon(k)-\mu(r)}{k_B T(r)})} \quad \text{(Equation 38)}$$

where ε , μ , , k_B , T are the electron energy, chemical potential, Boltzmann constant, and absolute temperature respectively. When there are no outside influences, the distribution function remains unchanged. However, when subjected to extraneous influences like a temperature gradient, electrons' locations and velocities shift at distinct intervals. The Boltzmann transport equation is difficult to solve exactly. The approximation of the relaxation time is used because of this [51].

$$\frac{\partial f}{\partial t} = \frac{f-f_0}{\tau} \quad \text{(Equation 39)}$$

As shown by Equation 39, once the external perturbation disappears, the distribution function (f) will revert to its equilibrium distribution. The approximation yields the following equations for the electrical conductivity (σ), electronic thermal conductivity (k_e), and Seebeck coefficient (S):

$$\sigma_{\alpha\beta}(T;\mu) = \frac{1}{\Omega}\int \bar{\sigma}_{\alpha\beta}(\varepsilon)[-\frac{\partial f_{\mu}(T;\epsilon)}{\partial \varepsilon}]d\varepsilon \quad \text{(Equation 40)}$$

$$k_{\alpha\beta}(T;\mu) = \frac{1}{e^{2}\mathrm{T}\Omega}\int \bar{\sigma}_{\alpha\beta}(\varepsilon)(\varepsilon-\mu)^{2}[-\frac{\partial f_{\mu}(T;\epsilon)}{\partial \varepsilon}]d\varepsilon \quad \text{(Equation 41)}$$

$$S_{\alpha\beta}(T;\mu) = \frac{1}{e\,\mathrm{T}\Omega\sigma_{\alpha\beta}(T;\mu)}\int \bar{\sigma}_{\alpha\beta}(\varepsilon)(\varepsilon-\mu)\,[-\frac{\partial f_{\mu}(T;\epsilon)}{\partial \varepsilon}]d\varepsilon \quad \text{(Equation 42)}$$

$$\sigma_{\alpha\beta}(T;\mu) = \frac{e^{2}}{N_{k}}\sum_{i,k}\tau\, v_{\alpha}\left(i,\vec{k}\right) v_{\beta}\left(i,\vec{k}\right)\frac{\delta(\varepsilon-\varepsilon_{i,\vec{k}})}{d\varepsilon} \quad \text{(Equation 43)}$$

Where, α, β, Ω, v, and N_k are the tensor components, chemical potential, unit cell volume, electron group velocity, and number of K points, respectively.

4. Chapter Four: Quaternary Heusler Alloy

First-principal Investigations of the Electronic, Magnetic, and Thermoelectric Properties of CrTiRhAl Quaternary Heusler Alloy

Abstract

Density functional theory (DFT) calculations were performed to investigate the electronic, magnetic, and thermoelectric properties of CrTiRhAl quaternary Heusler alloy (QHA). The type-I atomic configuration was found to be the most stable structure of this alloy. The CrTiRhAl QHA was also found to exhibit a semiconducting behavior with an indirect narrow gap of 0.129 eV at the majority spin channel. On the other hand, the minority spin channel exhibits a metallic behavior. The QHA has a total magnetic moment of 2 μ_B and 100% spin-polarization that making it ideal for potential spintronic applications. The Seebeck coefficient, electrical conductivity, and electronic thermal conductivity of CrTiRhAl alloy were calculated using the semi-classical Boltzmann theory. Additionally, the lattice thermal conductivity was predicted using Slack's equation. The calculations predicted a low figure of merit (*ZT*) below the Curie temperature, namely 0.4 at 300 K, which can be enhanced by lowering the structural dimensionality or doping for possible thermoelectric applications. However, the ZT value dropped drastically beyond Curie temperature (0.02 at 800K).

Keywords: Quaternary Heusler alloy, magnetic properties, lattice thermal conductivity, thermoelectrc properties.

1. Introduction:

Since the discovery of Heusler alloys in 1903, they have received much attention because of their interesting phenomena[52]. Heusler alloys show many functional properties that range from magnetoelastic couplings, shape memory, magnetic super elastic, magnetocaloric, and barcaloric effects [42, 43]. Their exciting features make them suitable for energy harvesters, sensors, actuators, and magnetic cooling devices. Heusler alloys can be half-metallic, where the band structure of one spin channel behaves as a metal, while the other spin channel has a semiconducting performance[17, 53]. The half-metallic behavior of these alloys leads to a complete spin polarization of the conduction electrons[54]. Besides the half-metallic character, diluted magnetic semiconductors are essential for spintronic materials. Heusler alloys are promising for thermoelectric applications because of their high Curie temperatures and narrow band gaps. They also have a high Seebeck coefficient and electrical conductivity corresponding to a high thermoelectric power factor. The values of the dimensionless figure-of-merit ($ZT = S^2\rho^{-1}\kappa^{-1}T$) of some Heusler compounds are close to those of cutting-edge thermoelectric materials [25].

A high *ZT* value of thermoelectric materials would result in improving their thermoelectric conversion efficiency [55]. Some Heusler alloys and their thermoelectric characteristics, including electrical conductivity, Seebeck coefficient, thermal conductivity, power factor, and *ZT* are very promising for thermoelectric applications [56]. The TE materials can be classified into different categories based on their *ZT* values: inefficient materials (ZT < 1), TE materials that can capture waste heat (ZT ≈ 2), and TE materials that can match the efficiency of modern refrigerators (ZT > 4). Therefore, the primary goal is to increase the ZT value of the TE material to the limit of efficient applications [38, 57].

Based on their chemical composition, Heusler alloys are classified into four types: Full Heusler alloys (FHA), Half-Heusler alloys (HHA), Quaternary-Heusler alloys (QHA), and Inverse Heusler alloys (IHA) [58]. Both FHA and IHA are composed of four interpenetrating FCC sublattices with the same chemical formula of X_2YZ, where X and Y are transitional metals (or Y can be a rare-earth atom), and Z is an s-p element from the leading group. However, in the case of FHA, the valence electrons of the Y transition-metal atom are less than the valence electrons of the X transition-metal atom. On the other hand, the valence electrons of the Y transition-metal are higher than those of the X atom in the case of IHA. The absence of one FCC lattice leads to the structure of HHA with the chemical formula XYZ. Finally, the QHA with the chemical formula X X`YZ is formed by replacing one of the X transition metal atoms by another (X`) in the full Heusler compound, where Y atom has less valence electrons than X` and the latter has less valence electrons than X.

The QHAs with their Y-type (LiMgPdSb-type) crystal structure and a space group of $F\bar{4}3m$ have received much attention recently because of their potential applications in technologies like spintronics, giant magnetoresistance devices, shape memory alloys, and thermoelectric devices. For example, Saadi Berri predicted a half-metallic ferromagnetic structure with an integer total magnetic moment value of $3\mu_B$ for CoMnCrSb QHA [59]. In addition, a theoretical and experimental study of NiCoMnAl, NiCoMnGe, and NiCoMnSn QHAs was carried out by Madhumita Halder *et al.* [60]. In their study, they found that the three QHAs have high Curie temperatures above 583K where only NiCoMnAl QHA has a nearly half-metallic ferromagnetic structure [60]. Moreover, Khodami and Ahmadian [15] predicted a half-metallic ferromagnetic behavior with a total magnetic moment value of $1\mu_B$ for CoMnTiP, CoMnTiAs, and CoMnTiSb QHAs. Elahmar *et al.* [16] found half metallic ferromagnetism in CoFeMnSi and

CoFeMnAs compounds with a magnetic moment of 4.02 and 4.99 Bohr magnetons, respectively. A similar trend of 100% spin polarization was observed in compounds CoRhMnGe and CoRhMnSi with a high Curie temperature of 928K in both the compounds [61]. Other prominent examples of half metallic FM QHAs in literature are CoNiMnSi [62], CoFeCrZ (Z = P, As, Sb) [63], ScNiCrZ (Z = Ga, Al, In) [64] and RhZrTiAl [65]. In addition, there are extensive studies of the thermoelectric properties of the QHAs. For example, the power factor (PF) values of 1.55×10^{12} $WK^{-2}m^{-1}s^{-1}$ and 1.38×10^{12} $WK^{-2}m^{-1}s^{-1}$were predicted for CoCuZrGe and CoCuZrSn QHAs, respectively [66]. Furthermore, first principal calculations indicated a high Seebeck coefficient and PF of 539.20μV/K and 7×10^{12} $mWK^{-2}m^{-1}s^{-1}$ for ZnFeTiSi, respectively [67]. In addition, promising ZT values of 0.71 and 0.61 were predicted for CoFeCrGe and CoFeTiGe QHAs, respectively [68]. Owing to their interesting properties, Heusler alloys have been extensively investigated. Fu *et al*. [8] predicted the maximum ZT value of FeNbTiSb QHA to be 1.1 at 1100 K, which is interesting for high temperature applications.

Many studies showed positive outcomes when looking more closely at Cr-based Heusler alloys. For example, Saadi Berri [13] predicted a half-metallic ferromagnetic structure with an integer total magnetic moment value of $3\mu_B$ for CoMnCrSb QHA. In a peer study, the spin polarization of Cr-based full-Heusler alloys is found to be higher than 90%. For example, the spin polarization of Co_2CrAl is 99.9%, Co_2CrSi is 100%, Co_2CrSn is 91.5%, and Co_2CrGa is 93.2%[69], which is favorable for spintronic devices. Also in another study for Cr-based HA, the ordered phase is discovered to be a compensated ferrimagnet with a vanishing magnetic moment, which agrees perfectly with the experimental finding [70].

The main aim of this study is to present a novel combination of QHA, CrTiRhAl. First the structural, dynamical, thermodynamical and mechanical stability of the QHA are studied to

investigate the feasibility of synthesizing this compound experimentally. These investigations were followed by the calculations of the electronic, magnetic and thermoelectric properties of CrTiRhAl QHA. The results show that CrTiRhAl is a promising candidate for spintronics applications. To the best of our knowledge there are no studies on this alloy. The rest of the paper is organized as follows: Section 2 describes the computational methodology, section 3 presents the results and discussions, and section 4 is devoted to the conclusions.

2. Method of Calculations

The calculations are performed using density functional theory (DFT). The structural optimizations were carried out using the projector augmented wave (PAW) method [71] as implemented in the Vienna ab initio simulation package (VASP) code [10]. The plane waves were stretched up to a cut-off energy of 520 eV with a total energy tolerance of 10^{-8}eV. The Brillouin zone integration for the unit-cell structures was constructed with a 22×22×22 k-point mesh for total energy calculations. The phonon calculations were performed using a 4×4×4 supercell structure within the finite-displacement method (FDM), as implemented in the Phonopy package, with a displacement of 0.01 Å. [72]. The optimized parameters are then used to run total energy calculations based on the full-potential linearized augmented plane wave (FP-LAPW) method as implemented in the WIEN2k code [73]. Perdew–Burke–Ernzerhof Generalized Gradient Approximation (GGA-PBE) is used to treat the exchange-correlation potential[74]. Plane waves with a cut-off value of $K_{max}R_{MT}$=8.5 were used to characterize the wavefunctions in the interstitial region, where R_{MT} is the smallest atomic muffin tin radius and K_{max} is the maximum k vector in the plane wave expansion. The R_{MT} of Cr, Ti, Rh, and Al atoms are 2.4, 2.2, 2.0, and 1.9 atomic units (a.u.), respectively. Inside the muffin-tin spheres, the maximum angular momentum (l_{max})

was set to 10 and the Fourier expansion of the charge density (G_{max}) was truncated at 12 $(\mathrm{Ryd})^{-1}$. The total energy, charge density, and force convergence tolerances were set to 10^{-4} Ryd, 10^{-4} e, and 1mRy/a. u. respectively. Boltzmann transport theory, as implemented in the BoltzTrap code, was used to determine thermoelectric characteristics, such as the Seebeck coefficient, electrical conductivities, electronic thermal conductivity, and power factor [75]. These thermoelectric (TE) properties were calculated using Boltzmann transport equations (BTE) with a highly dense mesh of 50000 k points, which is equivalent to a 36 ×36 ×36 Γ- centered k-mesh. All TE calculations were performed within the constant relaxation time approximation.

3. Results and Discussions:

This section presents the structural, dynamical, mechanical, electronic, magnetic, and thermoelectric properties of the CrTiRhAl alloy.

3.1 Structural properties

CrTiRhAl QHA crystalizes in a face-centered cubic LiMgPdSn crystal structure (Y-type) with a space group $F\bar{4}3m$ (no.216). There are three possible atomic configurations for this form of the QHA based on the occupation the Wyckoff positions 4a (0, 0, 0), 4b (1/2, 1/2, 1/2), 4c (1/ 4, 1/4, 1/4), and 4d (3/4, 3/4, 3/4) by the X, X', Y, and Z atoms, see Table 2. The conventional energy-minimization approach predicted type-I structure with a lattice constant of 6.1023 Å to be the most stable atomic configuration of CrTiRhAl QHA (Table 3). This prediction is similar to previous calculations of CoFeMnZ (Z=Al, Ga, Si, Ge) [76]. The thermodynamic stability of the alloy was determined using the following formula[77]:

$$E_{form} = E_{tot} - (E_{Cr} + E_{Ti} + E_{Rh} + E_{Al}), \quad \text{(Equation 1)}$$

where E_{tot} refers to the total energy of the QHA per formula unit, whereas E_{Cr}, E_{Ti}, E_{Rh} and E_{Al} are the total energies per atom of the constituent elements in their bulk structures. In general, if the formation energy of an alloy has a negative value, the alloy is considered to be thermodynamically stable. Therefore, the negative E_{form} value of CrTiRhAl QHA indicates its thermodynamic stability, see Table 3, in agreement with other previous calculations of VTiRhZ(Z=Si, Ge, Sn) alloys [78].

Further, the thermodynamic stability is also checked using convex hull calculations performed with Open Quantum Materials Database (OQMD) [79]. The CrTiRhAl compound decomposes into ternary $TiAlRh_2$, binary AlRh, TiAl and $TiCr_2$ with a convex hull value of 0.088eV/atom which is less than 0.1 eV/atom [80]. Hence CrTiRhAl phase is thermodynamically stable although it is competing with a full Heusler compound $TiAlRh_2$.

Table 2: The three possible atomic configurations of the QHA.

Y-type	**4a** **(0, 0, 0)**	**4c** **(1/4, 1/4, 1/4)**	**4b** **(1/2, 1/2, 1/2)**	**4d** **(3/4, 3/4, 3/4)**
I	Cr	Ti	Rh	Al
II	Cr	Rh	Ti	Al
II	Rh	Cr	Ti	Al

Table 3: The lattice parameter (a) and the formation energy (E_{form}) for the three types of the QHA.

Structure Type	**Total Energy (eV)**	**Lattice Parameters (Å)**	E_{form} **(eV)**
Type-I	-13865.75	6.1023	-2.12
Type-II	-13865.657	6.2329	-2.01
Type-III	-13865.655	6.1770	1.55

3.2 Dynamical properties

To better understand the dynamical stability of the investigated system, the phonon dispersion curve (PDC) was calculated using the PHONOPY package as implemented in VASP code [81]. Figure 4 depicts the PDC in the first Brillouin zone along the high-symmetry *k*-path (*W*-*L*-*X*-*W*). The dynamical characteristics are derived by solving the following eigenvalue problem within the harmonic approximation [65]:

$$D(q)e_{qj} = \omega_{qj}^2 e_{qj} \qquad \text{(Equation 2)}$$

Where, the dynamical matrix D(q) is calculated using the following relation:

$$D_{kk'}^{\alpha\beta}(q) = \sum_{l'} \frac{\Phi_{\alpha\beta}(ok,l'k')}{\sqrt{m_k m_k'}} e^{iq.[r(l'k'-r(ok)]} \qquad \text{(Equation 3)}$$

Where, m_k is the mass of the atom, $\omega_{qj}$is phonon frequency and e_{qj} is polarization vector and $\Phi_{\alpha\beta}$ is second order force constant (l and k are labels of unit cells and atoms, respectively) [65].

If any atomic displacements result in an increase in potential energy, then the crystal is dynamically stable. For the purposes of the harmonic approximation, this is mapped into actual (positive) frequencies for phonon dispersion relations.

The graph shows no imaginary (negative) frequencies, indicating that this alloy is dynamically stable. CrTiRhAl QHA has four atoms in the unit cell, which correspond to twelve frequency branches. They are three acoustic (at lower frequency) and nine optical branches (at higher frequency). The three acoustic branches consist of one longitudinal (LA) and two transverse (TA) branches. The overlap between the acoustic modes and the lower optical modes indicates higher phonon scattering rates, which leads to a low thermal conductivity.

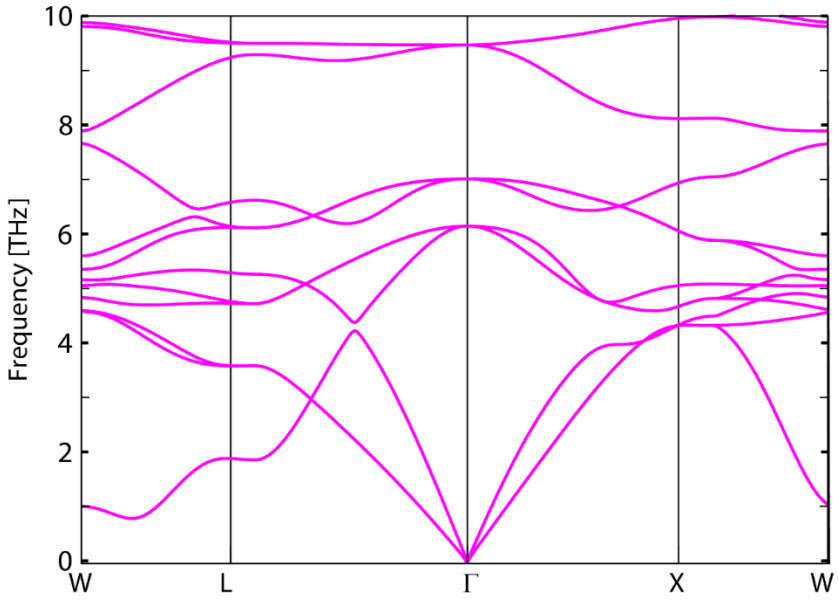

Figure 4: The phonon dispersion curves (PDCs) of CrTiRhAl.

3.3 Mechanical properties

The mechanical stability of materials can be inferred from the calculations of their elastic constants that relate the stress and the train using Hook's law as follows:

$$\sigma_{ij} = C_{ijkl}\varepsilon_{ij} \quad \text{(Equation 4)}$$

Where σ_{ij} is the stress tensor, ε_{ij} is the strain tensor and C_{ijkl} is the fourth order tensor or the proportionality coefficients, which are constants independent of the stress or the strain of the material. The fourth-suffix tensor C_{ijkl} can be converted to a two-suffix tensor C_{ij} by combining the first two suffices *i* and *j* into a single suffix *i* and the last two *k* and *l* into *j*. Similarly, the two-suffix tensors σ_{ij} and ε_{ij} become σ_i and ε_j. Here we have six-dimensional σ_i and ε_j and 6×6 C_{ij} matrix (*i* and *j*=1 to 6) vectors, where 1= *xx*, 2=*yy*, 3= *zz*, 4= *yz*, 5= *xz*, and 6= *xy*.

Here the CrTiRhAl QHA has a cubic structure, which leads to three independent elastic constants, the longitudinal compression(C_{11}), transverse expansion(C_{12}), and shear modulus predictor(C_{44}). The cubic structure is mechanically stable if the lattice constants satisfy the Born-Huang criteria as follows [82]:

$$C_{44} > 0, (C_{11}, - C_{12})/2 > 0, (C_{11}, + 2C_{12})/3 > 0. \quad \text{(Equation 5)}$$

These three conditions are satisfied for the case of CrTiRhAl QHA as shown in Table 3, which means that this alloy is mechanically stable.

As a result, various mechanical parameters, such as the bulk modulus (B), Voigt-Riess shear modulus (G), Young's moduli (E), anisotropy factor (A), Pugh ratio (B/G), and Cauchy pressure (C_P), can be calculated using the three elastic constants, see Table 4.

According to its definition, the bulk modulus (B) determines the material's resistance to compressions, which is given as follows:

$$B = \frac{(C_{11}+2C_{12})}{3} \quad \text{(Equation 6)}$$

From Table 3, the B value of CrTiRhAl QHA is 168.944 GPa. The shear modulus (G) explains how the shape changes when it experiences a force. It is known as the average of Voigt's (G_V) and Reuss's shear (G_R) moduli, which are defined as follows:

$$G = \frac{(G_V + G_R)}{2} \quad \text{where} \quad G_V = \frac{C_{11} - 2C_{12} + C_{44}}{5} \quad \text{and} \quad G_R = \frac{(5C_{44}(C_{11} - C_{12}))}{4C_{44} + 3(C_{11} - C_{12})} \quad \text{(Equation 7)}$$

The predicted G value is found to be 80.597 GPa. Furthermore, Young's modulus (E) is a measure of a material's stiffness, which is dependent on G and B values as follows:

$$E = \frac{9GB}{3B + G} \quad \text{(Equation 8)}$$

The value of E was calculated to be 208.50. The Poisson's ratio (V) is measured to check the compressibility of a material and its bonding force properties, which are determined as follows:

$$V = \frac{3B - 2G}{2(3B + G)} \quad \text{(Equation 9)}$$

The materials are more stable against external deterioration and less compressible if Poisson's ratio is in the range of 0.25–0.5. For a value outside this range, the materials become significantly more compressible [83-85]. The Poisson's ratio of CrTiRhAl QHA is 0.29, indicating that this alloy is ductile. In addition, the Pugh's ratio B/G and Cauchy pressure are obtained to be 2.09 and 27.74, respectively. Our results confirm the ductility of this alloy because of a positive Cauchy pressure value [86, 87].

The anisotropic ratio (A) was calculated to determine whether or not a material is isotropic or anisotropic in nature, which is calculated using the following equation [88]:

$$A = \frac{2C_{44}}{C_{11} - C_{12}} \quad \text{(Equation 10)}$$

Generally, if the alloy has A less than 1, it is considered anisotropic otherwise it is isotropic. According to our calculations, the anisotropy ratio of CrTiRhAl QHA is 0.73, which is less than unity (A < 1), indicating that CrTiRhAl QHA is anisotropic.

The heat resistance of a material is determined by its melting temperature, which can be calculated using the equation below [87]:

$$T_{melt} = [553\ \text{K} + (5.91\ \text{K/ GPa})\ C_{11}\ ] \pm 300\ \text{K} \quad \text{(Equation 11)}$$

The melting point value of CrTiRhAl is 2278 K, which is higher than other that QHAs such as CoFeMnGe (1450 K) [36]. The mechanical stability of QHA may be inferred from the relatively high values of the melting temperature [78].

Table 4: The elastic constants (C_{ij}) of CrTiRhAl

Alloy	C_{11} (GPa)	C_{12} (GPa)	C_{44} (GPa)	**B** (GPa)	**G** (GPa)	**E**	**V**	**B/G**	C_p (GPa)	**A**	T_{melt} (K)
CrTiRhAl	292.02	98.97	71.22	168.94	80.5	208.52	0.29	2.09	27.74	0.73	278

3.4 Electronic properties

The electrical and magnetic characteristics of a crystal are determined by its structural arrangement, with various atomic orders exhibiting different electronic and magnetic properties for the same compound [76]. The band structures, the total density of states (TDOS), and the projected density of states (PDOS) of CrTiRhAl QHA are shown in Figure 5. The majority-spin band structure shows a semiconducting behavior with a band gap of 0.129 eV, while the minority-spin band structure exhibits a metallic behavior. This behavior on is referred to as a half metallicity [89]. The majority-spin band structure of CrTiRhAl QHA is found to be direct at the Γ high symmetry point. Having a direct bandgap is desired for high-power electronics and high-temperature applications[90]. Our findings are in fair agreement with other theoretical calculations of VTiRhZ(Z=Al, Ga, In) [30]. Figure 5 presents also the TDOS, which reflects the half-metallic behavior as the minority-spin channel has electronic states at the Fermi level, which are absent in the case of the majority-spin channel.

The origin of the bandgap can be explained by the *d-d* hybridization of the constituent transition metals [91, 92]. A schematic diagram of the *3d*-orbitals is depicted in Figure (6a) located near the Fermi energy level (E_F). The s-orbital and triply degenerate p –orbitals of Al atom are way below the Fermi energy level (as evident from the PDOS) and are ignored in the schematics. The two-fold degenerate sub-levels of the d orbital of Cr atom, namely d_{z^2} and $d_{x^2-y^2}$, hybridize with that of Rh atoms forming bonding e_g and antibonding e_u states, while the d_{xy} d_{yz} and d_{zx} orbitals of both the atoms hybridize to form bonding t_{2g} and anti-bonding t_{1u} states. Here e_u and e_g states are doubly degenerate whereas t_{2g} and t_{1u} states are triply degenerate. In the figure (6b), the total 5 bonding e_g and t_{2g} states formed by Cr-Rh hybridization will hybridize with 5 d-orbitals of Ti producing 5 bonding and 5 antibonding orbitals, thus giving rise to 15x hybridized d-orbitals. The Fermi Energy is located between anti-bonding e_u and t_{1u} states. There are 8x occupied hybridized d-orbitals and hence the Slater-Pauling rule will be Mt = 24-Z_t. Z_t is the number of valence electrons – there are 6 per Cr atom, 4 per Ti atom, 9 per Rh atom and 3 per Al atom making a total Zt=22. Hence, net magnetic moment is 2 Bohr magnetons.

Figure 7 presents the projected density of states (PDOS). This figure shows that the valence band of CrTiRhAl QHA has two main regions. The Rh-*d* orbital shows the main contribution in the region from -4 eV to -2 eV, whereas, the contributions of Ti and Cr *d*- orbitals as well as Al *p*-orbitals are very small in both the majority and minority spin channels. However, the region between -2 eV to the Fermi level shows the most contribution from Cr *d*-orbital in the majority spin channel. In contrast, the minority spin channel has a mixture of different orbitals. The *d*-orbital of Cr, Ti, and Rh shows the most significant contribution in the conduction band for CrTiRhAl QHA.

The spin polarization of the alloy is obtained by using the following equation [93]:

$$P = \frac{\rho_{\text{majority}}(E_f) - \rho_{\text{minority}}(E_f)}{\rho_{\text{majority}}(E_f) + \rho_{\text{minority}}(E_f)} \times 100, \qquad \text{((Equation 12)}$$

where $\rho_{\text{majority}}\left(E_f\right)$ and $\rho_{\text{minority}}\left(E_f\right)$ refer to the majority and minority spin density of states at the Fermi level E_f, respectively[93-95]. A perfect half-metallicity of 100% spin polarization was obtained due to the absence of the density of states at the Fermi level E_f in the majority spin channels (Table 5).

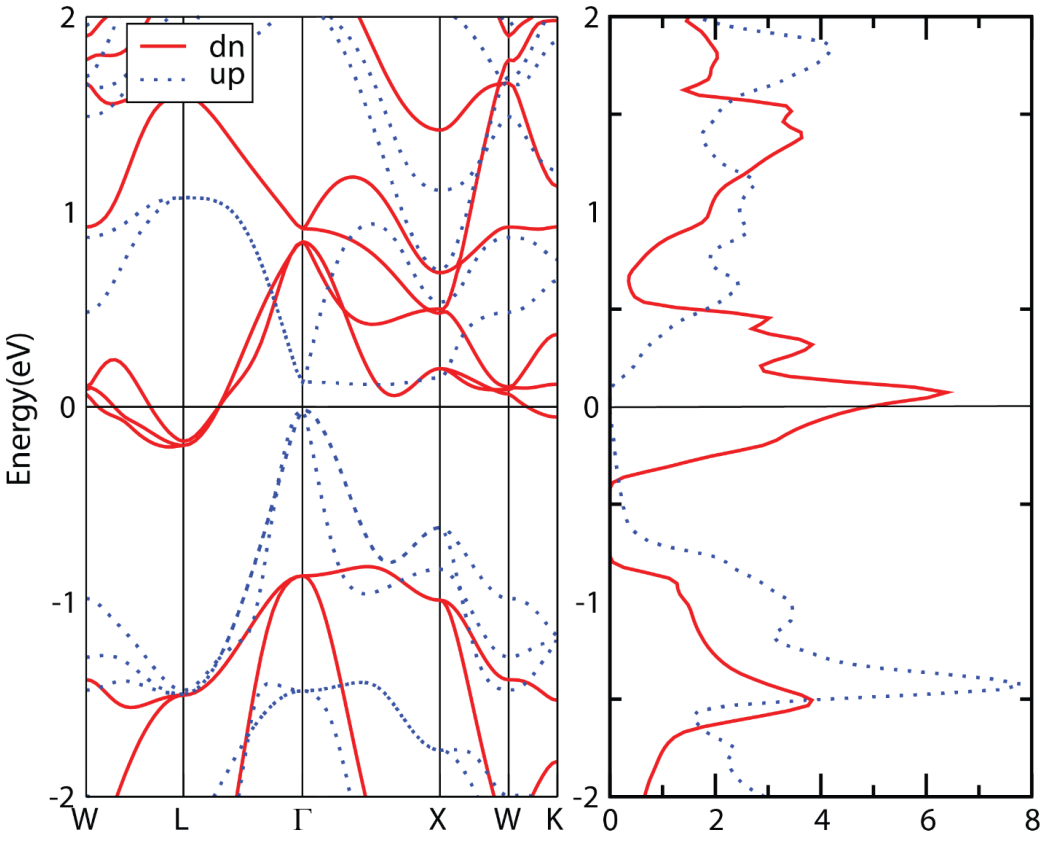

Figure 5: The electronic band structures and total density of states (TDOS) of a CrTiRhAl.

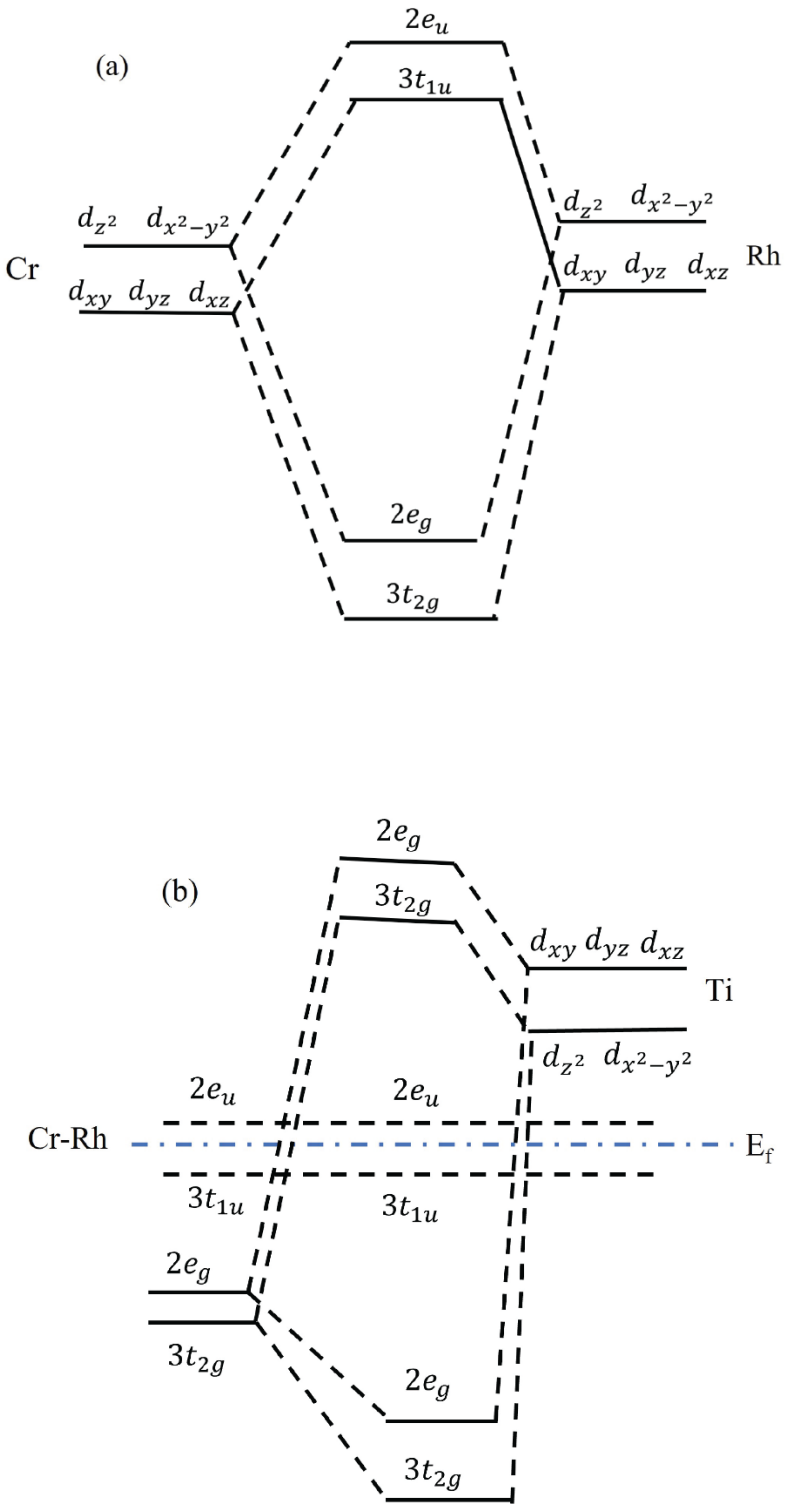

Figure 6:Schematic diagram of the 3d-orbitals located near the fermi energy level (EF) of CrTiRhAl.

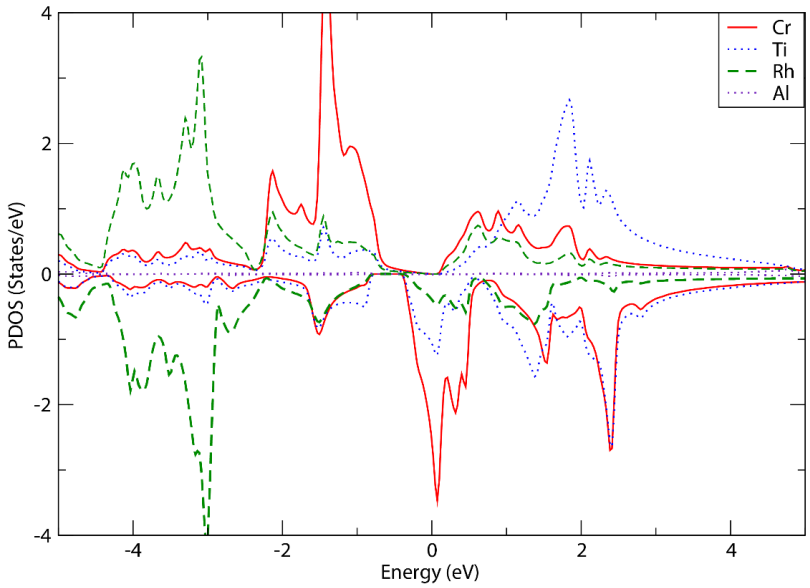

Figure 7: The projected density of state (PDOS) of CrTiRhAl.

Table 5: The band gap (Eg), total magnetic moment (M_tot), interstitial magnetic moment (Minit) and local magnetic moments (Mi; i=Cr, Ti, Ph, and Al). of CrTiRhAl QHA.

Alloy	**E_g (eV)**	**P %**	**M_{tot} (μ_B)**	**M_{init} (μ_B)**	**M_{Cr} (μ_B)**	**M_{Ti} (μ_B)**	**M_{Rh} (μ_B)**	**M_{Al} (μ_B)**
CrTiRhAl	**0.129**	**100**	**2**	**0.11541**	**2.0626**	**-0.2465**	**0.0843**	**-0.0158**

3.5 Magnetic properties

This subsection presents the magnetic properties of the CrTiRhAl QHA. According to the slater-Pauling equation, a half-metallic material has an integer value of the total magnetic moment [23, 96], which is defined as follows:

$$M_{\text{tot}} = N_{\text{majority}} - N_{\text{minority}} = (Z_{\text{tot}} - N_{\text{minority}}) - N_{\text{minority}} = Z_{\text{tot}} - 2N_{\text{minority}}. \quad \text{(Equation13)}$$

Here, the M_{tot} , N_{majority}, N_{minority}, and Z_{tot} are the total magnetic moment, the majority spin valence electrons, the minority spin valence electrons, and the total valence electron number, respectively. For CrTiRhAl QHA, the total magnetic moment is 2 μB see Table 4. This is similar to DFT value of the net magnetic moment as shown in Table 4. The major contribution to the net magnetic moment comes from Cr atom. The negative magnetic moments of Ti and Al implies that they are coupled antiferromagnetically with the lattice. This result agrees with previous first-principal calculations of a similar QHA, namely VTiRhSi [78].

One approach for estimating the Curie temperature is by using the linear relationship between the Curie temperature (T_C) and the total magnetic moments, as shown in the following equation [78]:

$$T_C = 23 + 181\ M_{\mathrm{tot}} \qquad \text{(Equation 14)}$$

The CrTiRhAl QHA has a Curie temperature of 385 K, which is similar to other calculations of CoFeCrAs (378K) and CoFeCrSb (360K)[97]. This result is higher than the room temperature, making it an excellent candidate for QHAs in spintronics applications.

3.6 Thermoelectric properties

The thermoelectric properties of CrTiRhAl QHA are calculated in this subsection using the semiclassical Boltzmann transport equations (BTE) theory [98]. This theory is used to compute the values of the Seebeck coefficient (S), electrical conductivity (σ/τ), and the Electrical conductivity (κ_e). Narrow band gap semiconductors are predicted to have promising thermoelectric features [99]. The thermoelectric properties include: Seebeck coefficient, electronic and lattice thermal conductivity, and figure of merit, which are interdependent.

The figure of merit (*ZT)* of a thermoelectric material is defined as follows:

$$ZT = \frac{S^2\sigma}{\kappa_e+\kappa_l} \quad \text{(Equation 15)}$$

While the transport parameters, *S*, σ , and κ_e are calculated using Boltzmann transport theory, κ_l is calculated using Slack's equation as follows [100]:

$$\kappa_l = A\frac{\bar{M}\Theta_D^3 V^{1/3}}{\gamma^2 n^{2/3} T} \quad \text{(Equation 16)}$$

$$A = \left(\frac{2.43\times10^{-6}}{1-\frac{0.514}{\gamma}+\frac{0.228}{\gamma^2}}\right) \quad \text{(Equation 17)}$$

where $\bar{M}$ is the average atomic mass, Θ_D is the acoustic phonon mode Debye-temperature, *V* is the volume per atom, γ is Grüneisen parameter, *n* is the number of atoms in the primitive unit cell, and *T* is temperature. Figure 8 presents the κ_l as a function of temperature. One can notice that the κ_l decreases as the temperature increases. The κ_l value is found to be 4.73 $W.m^{-1}$ K^{-1}at 300K, which is less than other previous calculations for CoFeCrGe and CoFeTiGe QHAs [68].

The total Seebeck coefficient (a measure of a material's ability to generate voltage due to a temperature differential) for half-metallic materials can be calculated using the two current models as follows [101]:

$$S = (S\uparrow \sigma\uparrow + S\downarrow \sigma\downarrow) / \sigma_{total} \quad \text{(Equation 18)}$$

where S↑ (S↓) and σ↑ (σ↓) are the Seebeck coefficients and electrical conductivities of spin-up (spin-down) channels, respectively. The total electrical conductivity is represented as σ_{total} = (σ↑ + σ↓). Figure. 9 (a) presents the Seebeck coefficient (*S*) as a function of the chemical potential at 300 K, where the highest values are about 20 μV/K for the p-type doping and -40 μV/K for the n-type doping. The electrical conductivity per relaxation time (σ/τ) as a function of the chemical potential at 300K is depicted in Figure 9 (b). The results show that σ/τ value increases in the regions beyond the Fermi level due to the presence of holes (electrons) in the case of p-type (n-type) doping.

The electronic thermal conductivity per relaxation time (κ_e/τ) is shown in Figure 9 (c) as a function of the chemical potential at 300 K, which has a similar behavior as σ/τ. This behavior is due to the direct relation between κ_e and σ as per Wiedemann–Franz law [31]:

$$\kappa_e = L\sigma T. \quad \text{(Equation 19)}$$

Based on this relation, Our finding is in agreement with other calculations of CoFeCrGe and CoFeTiGe [68].

In general, a high ZT value indicates that the thermoelectric material has a high conversion efficiency. The ZT value can be enhanced by raising the Seebeck coefficient or electrical conductivity or decreasing the lattice thermal conductivity. Increasing the electrical conductivity, on the other hand, increases the electronic thermal conductivity. As a result, the best thermoelectric materials have ZT ≈ 1.0 [102]. In the present calculations, the relaxation time (τ) is set to the standard value of semiconductors (0.5×10^{-15}s) [103, 104]. The *ZT* value is presented in Figure 9(d) as a function of the chemical potential at 300K, where the highest *ZT* value is found to be 0.4. This value is higher than that of a similar study for CoFeTiGe QHA (0.15)[68]. Beyond the Curie temperature (358 K), CrTiRhAl QHA transfers into a metallic nonmagnetic material. For this case, the ZT is calculated at 800 K, which shows a very low value of 0.02. This finding indicates that CrTiRhAl QHA is not optimal for thermoelectric applications at higher temperatures. On the other hand, this material could be promising for thermoelectric applications at temperatures less than Curie temperature by means of doping or lowering its structural dimensionality, which may enhance the ZT values.

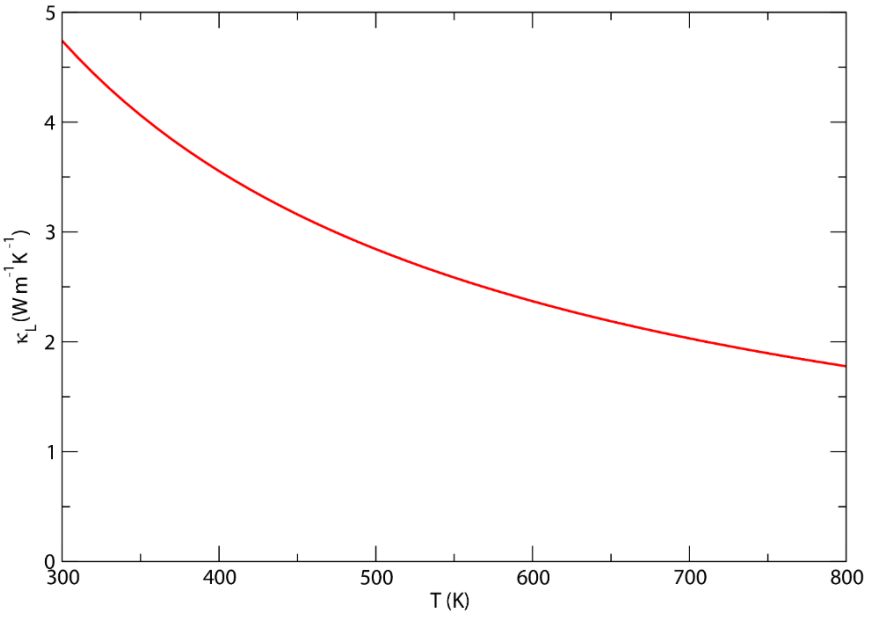

Figure 8: The lattice thermal conductivity as function temperature of CrTiRhAl.

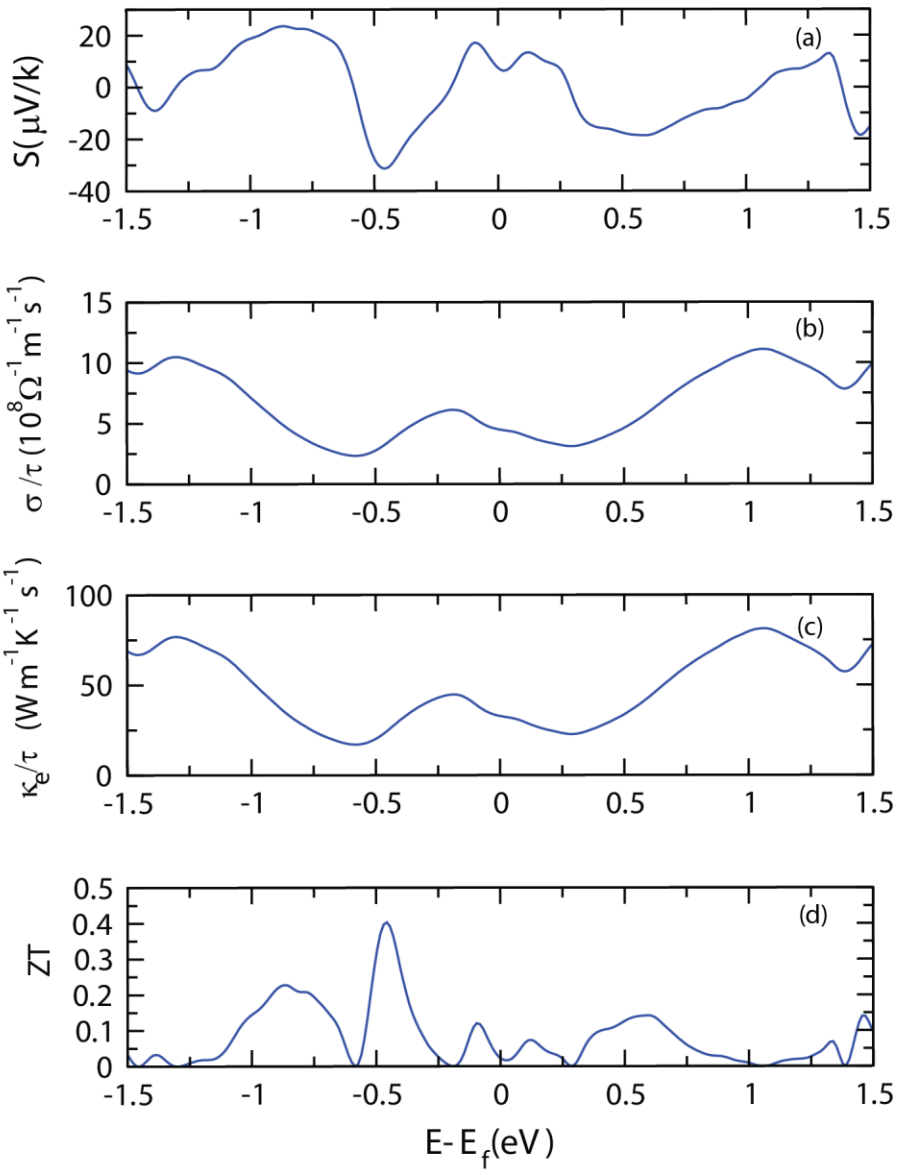

Figure 9: The Seebeck coefficient (S), electrical conductivity per relaxation time (σ/ τ), electronic thermal conductivity per relaxation time (κ_e/τ) and the figure of merit (ZT) of CrTiRhAl.

Conclusion

Density functional theory calculations are performed to investigate the structural, dynamical, mechanical, and electronic properties of CrTiRhAl QHA. The energy-minimization

calculations predicted the type-1 structure as the ground state configuration of CrTiRhAl QHA. The stability was then confirmed by the dynamic properties where the phonon dispersion curve of CrTiRhAl QHA shows no imaginary (negative) frequencies, which means that this compound is dynamically stable. In addition, CrTiRhAl QHA mechanical properties stability were confirmed by calculating the elastic constants, Cij. The melting point (T_{melt}), Voigt-Riess shear modulus (*G*), and bulk modulus (*B*) of CrTiRhAl are found to be 2278 K, 80.597 GPa, and 168.944 GPa, which all confirm the mechanical stability of the compound. The electronic and magnetic investigations show that the CrTiRhAl QHA possesses a half-metallic nature with a narrow band gap of 0.129 eV in the majority spin channel, whereas the minority spin channel is metallic. The QHA has a total magnetic moment of 2 μ_B and 100% spin-polarization, which is promising for spintronic applications. The thermoelectric transport parameters were obtained using Boltzmann transport theory, whereas κ_l was predicted using Slack's equation. The calculations show a reasonable *ZT* value of 0.4 at 300 K, which could be enhanced by doping or lowering the structural dimensiolty.

References

1. Yang, J. and F.R. Stabler, *Automotive applications of thermoelectric materials.* Journal of electronic materials, 2009. **38**(7): p. 1245.

2. Kumar, A., et al., *A Review on Fundamentals, Design and Optimization to High ZT of Thermoelectric Materials for Application to Thermoelectric Technology.* Journal of Electronic Materials, 2021. **50**(11): p. 6037-6059.

3. Hooshmand Zaferani, S., et al., *Thermal Management Systems and Waste Heat Recycling by Thermoelectric Generators—An Overview.* Energies, 2021. **14**(18): p. 5646.

4. Celestin, S.-J., *Understanding the effect of Spin-state on the Seebeck Coefficient of Iron Doped Barium Titanate (Fe-BTO) via Molecular Beam Epitaxy for high-efficiency thermoelectric applications.* 2016.

5. Wang, N., et al., *A novel high-performance photovoltaic–thermoelectric hybrid device.* Energy & Environmental Science, 2011. **4**(9): p. 3676.

6. Yang, J. and T. Caillat, *Thermoelectric Materials for Space and Automotive Power Generation.* MRS Bulletin, 2006. **31**(3): p. 224-229.

7. Felser, C., G.H. Fecher, and B. Balke, *Spintronics: A Challenge for Materials Science and Solid-State Chemistry.* Angewandte Chemie International Edition, 2007. **46**(5): p. 668-699.

8. Jung, D., H.J. Koo, and M.H. Whangbo, *Study of the 18-electron band gap and ferromagnetism in semi-Heusler compounds by non-spin-polarized electronic band structure calculations.* Journal of Molecular Structure: THEOCHEM, 2000. **527**(1): p. 113-119.

9. Özdoğan, K., E. Şaşıoğlu, and I. Galanakis, *Slater-Pauling behavior in LiMgPdSn-type multifunctional quaternary Heusler materials: Half-metallicity, spin-gapless and magnetic semiconductors.* Journal of Applied Physics, 2013. **113**(19): p. 193903.

10. Sutou, Y., et al., *Magnetic and martensitic transformations of NiMnX(X=In,Sn,Sb) ferromagnetic shape memory alloys.* Applied Physics Letters, 2004. **85**(19): p. 4358.

11. Klimczuk, T., et al., *Superconductivity in the Heusler family of intermetallics.* Physical Review B, 2012. **85**(17).

12. Graf, T., et al., *Crystal structure of new Heusler compounds.* Zeitschrift für anorganische und allgemeine Chemie, 2009. **635**(6-7): p. 976-981.

13. Qin, G., et al., *Effect of swap disorder on the physical properties of the quaternary heusler alloy PdMnTiAl: A first-principles study.* IUCrJ, 2017. **4**(4): p. 506-511.

14. Haleoot, R.E., *Theoretical Investigations of the Electronic, Magnetic, and Thermoelectric Properties of Transition-Metal Based Compounds*. 2019, University of Arkansas: Ann Arbor. p. 125.

15. Amudhavalli, A., R. Rajeswarapalanichamy, and K. Iyakutti, *First principles study on Fe based ferromagnetic quaternary Heusler alloys.* Journal of Magnetism and Magnetic Materials, 2017. **441**: p. 21-38.

16. Alijani, V., et al., *Electronic, structural, and magnetic properties of the half-metallic ferromagnetic quaternary Heusler compounds CoFeMn Z (Z= Al, Ga, Si, Ge).* Physical Review B, 2011. **84**(22): p. 224416.

17. Gao, G.Y., et al., *Large half-metallic gaps in the quaternary Heusler alloys CoFeCrZ (Z=Al, Si, Ga, Ge): A first-principles study.* Journal of alloys and compounds, 2013. **551**: p. 539-543.

18. Kushwaha, V.K., et al., *Prediction of half-metallic gap formation and Fermi level position in Co-based Heusler alloy epitaxial thin films through anisotropic magnetoresistance effect.* Physical Review Materials, 2022. **6**(6): p. 064411.

19. Sefir, Y., et al., *Structural, electronic, magnetic and thermodynamic properties of the new multifunctional half-Heusler alloy CoTcSn: Half-metallic and ferromagnetic behaviour.* Pramana, 2021. **95**(2).

20. Bouferrache, K., et al., *Stability, electronic band structure, magnetic, optical and thermoelectric properties of CoXCrZ (X = Fe, Mn and Z = Al, Si) and FeMnCrSb quaternary Heusler.* Chinese Journal of Physics, 2022.

21. Marchenkov, V.V., V.Y. Irkhin, and A.A. Semiannikova, *Unusual Kinetic Properties of Usual Heusler Alloys.* Journal of Superconductivity and Novel Magnetism, 2022. **35**(8): p. 2153-2168.

22. Graf, T., S.S.P. Parkin, and C. Felser, *Heusler compounds—A material class with exceptional properties.* IEEE Transactions on Magnetics, 2010. **47**(2): p. 367-373.

23. Luo, H., et al., *Slater–Pauling behavior and half-metallicity in Heusler alloys Mn2CuZ (Z=Ge and Sb).* Computational materials science, 2011. **50**(11): p. 3119-3122.

24. Kim, H.S., et al., *Relationship between thermoelectric figure of merit and energy conversion efficiency.* Proceedings of the National Academy of Sciences - PNAS, 2015. **112**(27): p. 8205-8210.

25. Sofi, S.A. and D.C. Gupta, *Current research and future prospective of cobalt-based Heusler alloys as thermoelectric materials: A density functional approach.* International Journal of Energy Research, 2021. **45**(3): p. 4652-4668.

26. Chen, S. and Z. Ren, *Recent progress of half-Heusler for moderate temperature thermoelectric applications.* Materials today, 2013. **16**(10): p. 387-395.

27. Moore, J.P. and R.S. Graves, *Absolute Seebeck coefficient of platinum from 80 to 340 K and the thermal and electrical conductivities of lead from 80 to 400 K.* Journal of Applied Physics, 1973. **44**(3): p. 1174-1178.

28. Goldsmid, H.J. and R.W. Douglas, *The use of semiconductors in thermoelectric refrigeration.* British Journal of Applied Physics, 1954. **5**(11): p. 386.

29. Liu, Z., et al., *High thermoelectric performance of α-MgAgSb for power generation.* Energy & Environmental Science, 2018. **11**(1): p. 23-44.

30. Alqurashi, H., R. Haleoot, and B. Hamad, *First-principles investigations of the electronic, magnetic and thermoelectric properties of VTiRhZ (Z= Al, Ga, In) Quaternary Heusler alloys.* Materials Chemistry and Physics, 2022. **278**: p. 125685.

31. Alqurashi, H., et al., *Investigations of the electronic, dynamical, and thermoelectric properties of Cd1-xZnxO alloys: First-principles calculations.* Materials Today Communications, 2021. **28**: p. 102511.

32. Graf, T., S.S.P. Parkin, and C. Felser, *Heusler Compounds-A Material Class With Exceptional Properties.* IEEE transactions on magnetics, 2011. **47**(2): p. 367-373.

33. Skaftouros, S., et al., *Search for spin gapless semiconductors: The case of inverse Heusler compounds.* Applied Physics Letters, 2013. **102**(2): p. 022402.

34. Chinnadurai, K. and B. Natesan, *First principles calculations of 3d-4d transition metal based LiMgPdSn–type FeCrRuZ (Z = Al, Ga, In, Si) equiatomic quaternary Heusler alloys.* Computational Materials Science, 2021. **188**: p. 110116.

35. Fabian, K., V.P. Shcherbakov, and S.A. Mcenroe, *Measuring the Curie temperature.* Geochemistry, Geophysics, Geosystems, 2013. **14**(4): p. 947-961.

36. Bainsla, L., et al., *High spin polarization in CoFeMnGe equiatomic quaternary Heusler alloy.* Journal of Applied Physics, 2014. **116**(20): p. 203902.

37. Guo, R., et al., *First-principles study on quaternary Heusler compounds ZrFeVZ (Z = Al, Ga, In) with large spin-flip gap.* RSC Advances, 2016. **6**(111): p. 109394-109400.

38. Hamad, B., *Theoretical Investigations of the Thermoelectric Properties*

of Fe2NbGa1−x Al x(x = 0, 0.25, 0.5) Alloys. Journal of Electronic Materials, 2017.

39. Hamad, B., *Ab initio investigations of the structural, electronic, and thermoelectric properties of Fe2NbAl-based alloys.* Journal of materials science, 2016. **51**(24): p. 10887-10896.

40. Kangsabanik, J. and A. Alam, *Bismuth based half-Heusler alloys with giant thermoelectric figures of merit.* Journal of Materials Chemistry A, 2017. **5**(13): p. 6131-6139.

41. Jaishi, D.R., et al., *Rhodium-based half-Heusler alloys as thermoelectric materials.* Physical Chemistry Chemical Physics, 2022. **24**(33): p. 19844-19852.

42. Entel, P., et al., *Optimization of smart Heusler alloys from first principles.* Journal of Alloys and Compounds, 2013. **577**: p. S107-S112.

43. Hzzazi, A.H., *Theoretical Investigations of the Structural, Dynamical, Electronic, Magnetic, and Thermoelectric Properties of CoRhYSi (Y = Cr, Mn) Quaternary Heusler Alloys.*

44. Hartree, D.R., *The Wave Mechanics of an Atom with a Non-Coulomb Central Field. Part I. Theory and Methods.* Mathematical proceedings of the Cambridge Philosophical Society, 1928. **24**(1): p. 89-110.

45. Thomas, L.H. *The calculation of atomic fields*. Cambridge University Press.

46. Orio, M., D.A. Pantazis, and F. Neese, *Density functional theory.* Photosynthesis research, 2009. **102**(2): p. 443-453.

47. Kohn, W. and L.J. Sham, *Self-consistent equations including exchange and correlation effects.* Physical review, 1965. **140**(4A): p. A1133.

48. Perdew, J.P., K. Burke, and M. Ernzerhof, *Generalized gradient approximation made simple.* Physical review letters, 1996. **77**(18): p. 3865.

49. Ceperley, D.M. and B.J. Alder, *Ground state of the electron gas by a stochastic method.* Physical review letters, 1980. **45**(7): p. 566.

50. Csonka, G.I., et al., *Assessing the performance of recent density functionals for bulk solids.* Physical Review B, 2009. **79**(15): p. 155107.

51. Nag, B.R., *Electron transport in compound semiconductors*. Vol. 11. 2012: Springer Science & Business Media.

52. Hirohata, A., et al., *Heusler alloy/semiconductor hybrid structures.* Current Opinion in Solid State & Materials Science, 2006. **10**(2): p. 93-107.

53. Jia, L.Y., et al., *New Quaternary Half-Metallic Materials of the Z(t)-28 Rule in LiMgPdSn-Type Heusler Alloys.* Journal of Superconductivity and Novel Magnetism, 2018. **31**(4): p. 1067-1072.

54. Fang, C.M., G.A. de Wijs, and R.A. de Groot, *Spin-polarization in half-metals (invited).* Journal of Applied Physics, 2002. **91**(10): p. 8340-8344.

55. Fu, C., et al., *Band engineering of high performance p-type FeNbSb based half-Heusler thermoelectric materials for figure of merit zT > 1.* Energy & Environmental Science, 2015. **8**(1): p. 216-220.

56. Mastronardi, K., et al., *Antimonides with the half-Heusler structure: New thermoelectric materials.* Applied physics letters, 1999. **74**(10): p. 1415-1417.

57. Zheng, X.F., et al., *A review of thermoelectrics research – Recent developments and potentials for sustainable and renewable energy applications.* Renewable & sustainable energy reviews, 2014. **32**: p. 486-503.

58. Seh, A.Q. and D.C. Gupta, *Quaternary Heusler alloy <scp>CoZrMnAs</scp> competent candidate for spintronics and thermoelectric technologies.* Energy Storage, 2022.

59. Berri, S., *First-principles Study on Half-metallic Properties of the CoMnCrSb Quaternary Heusler Compound.* Journal of Superconductivity and Novel Magnetism, 2016. **29**(5): p. 1309-1315.

60. Halder, M., et al., *Electronic, structural, and magnetic properties of the quaternary Heusler alloy NiCoMnZ (Z=Al, Ge, and Sn).* Journal of Magnetism and Magnetic Materials, 2015. **377**: p. 220-225.

61. Benkabou, M., et al., *Electronic structure and magnetic properties of quaternary Heusler alloys CoRhMnZ (Z = Al, Ga, Ge and Si) via first-principle calculations.* Journal of Alloys and Compounds, 2015. **647**: p. 276-286.

62. Elahmar, M.H., et al., *Structural stability, electronic structure and magnetic properties of the new hypothetical half-metallic ferromagnetic full-Heusler alloy CoNiMnSi.* Materials Science-Poland, 2016. **34**(1): p. 85-93.

63. Gharbi, F.N., et al. *Theoretical Studies of the Structural, Electronic and Magnetic Properties of the CoFeCeZ (Z= P, As and Sb) Quaternary Heusler Alloys*. World Scientific.

64. Rabah, I.E., et al. *A Theoretical Analysis of Physical Properties and Half-Metallic Stability under Pressure Effect of the ScNiCrZ (Z= Ga, Al, In) Heusler Alloys*. World Scientific.

65. Rached, H., *Prediction of a new quaternary Heusler alloy within a good electrical response at high temperature for spintronics applications: DFT calculations.* International Journal of Quantum Chemistry, 2021. **121**(12): p. e26647.

66. Mushtaq, M., M.A. Sattar, and S.A. Dar, *Phonon phase stability, structural, mechanical, electronic, and thermoelectric properties of two new semiconducting quaternary Heusler alloys CoCuZrZ (Z = Ge and Sn).* International Journal of Energy Research, 2020. **44**(7): p. 5936-5946.

67. Lin, T.T., et al., *Dynamical stability, electronic and thermoelectric properties of quaternary ZnFeTiSi Heusler compound.* Current Applied Physics, 2019. **19**(6): p. 721-727.

68. Haleoot, R. and B. Hamad, *Thermodynamic and thermoelectric properties of CoFeYGe (Y = Ti, Cr) quaternary Heusler alloys: first principle calculations.* Journal of physics. Condensed matter, 2019. **32**(7): p. 075402-075402.

69. Rai, D.P. and R.K. Thapa, *An abinitio study of the half-metallic properties of Co2TGe (T= Sc, Ti, V, Cr, Mn, Fe): LSDA+ U method.* Journal of the Korean Physical Society, 2013. **62**(11): p. 1652-1660.

70. Jamer, M.E., et al., *Low-moment ferrimagnetic phase of the Heusler compound Cr2CoAl.* Journal of Magnetism and Magnetic Materials, 2015. **394**: p. 32-36.

71. Kresse, G. and D. Joubert, *From Ultrasoft Pseudopotentials to the Projector Augmented-Wave Method.* Physical review. B, Condensed matter, 1999. **59**(3): p. 1758-1775.

72. Kresse, G. and J. Hafner, *Ab initio molecular-dynamics simulation of the liquid-metal-amorphous-semiconductor transition in germanium.* Physical review. B, Condensed matter, 1994. **49**(20): p. 14251-14269.

73. Blaha, P., et al., *Full-potential, linearized augmented plane wave programs for crystalline systems.* Computer physics communications, 1990. **59**(2): p. 399-415.

74. Perdew, J.P., K. Burke, and M. Ernzerhof, *Generalized Gradient Approximation Made Simple [Phys. Rev. Lett. 77, 3865 (1996)].* Physical review letters, 1997. **78**(7): p. 1396-1396.

75. Madsen, G.K.H., D.J. Singh, and O.R.T.N. Oak Ridge National Lab, *BoltzTraP. A code for calculating band-structure dependent quantities.* Computer physics communications, 2006. **175**(1): p. 67-71.

76. Alijani, V., et al., *Electronic, structural, and magnetic properties of the half-metallic ferromagnetic quaternary Heusler compounds CoFeMnZ(Z=Al, Ga, Si, Ge).* Physical review. B, Condensed matter and materials physics, 2011. **84**(22).

77. Haleoot, R. and B. Hamad, *Ab Initio Investigations of the Structural, Electronic, Magnetic, and Thermoelectric Properties of CoFeCuZ (Z = Al, As, Ga, In, Pb, Sb, Si, Sn) Quaternary Heusler Alloys.* Journal of electronic materials, 2018. **48**(2): p. 1164-1173.

78. Alqurashi, H. and B. Hamad, *Magnetic structure, mechanical stability and thermoelectric properties of VTiRhZ (Z = Si, Ge, Sn) quaternary Heusler alloys: first-principles calculations.* Applied physics. A, Materials science & processing, 2021. **127**(10).

79. Kirklin, S., et al., *The Open Quantum Materials Database (OQMD): assessing the accuracy of DFT formation energies.* npj Computational Materials, 2015. **1**(1): p. 1-15.

80. Gao, Q., I. Opahle, and H. Zhang, *High-throughput screening for spin-gapless semiconductors in quaternary Heusler compounds.* Physical Review Materials, 2019. **3**(2): p. 024410.

81. Kresse, G. and J. Hafner, *Ab initio molecular dynamics for liquid metals.* Physical review. B, Condensed matter, 1993. **47**(1): p. 558-561.

82. Surucu, G., et al., *Investigation of structural, electronic, magnetic and lattice dynamical properties for XCoBi (X: Ti, Zr, Hf) Half-Heusler compounds.* Physica. B, Condensed matter, 2020. **587**: p. 412146.

83. Lee, T. and R.S. Lakes, *Anisotropic polyurethane foam with Poisson'sratio greater than 1.* Journal of materials science, 1997. **32**(9): p. 2397-2401.

84. Candan, A., *Magnetic, Electronic, Mechanic, Anisotropic Elastic and Vibrational Properties of Antiferromagnetic Ru2TGa (T = Cr, Mn, and Co) Heusler Alloys.* Journal of electronic materials, 2019. **48**(12): p. 7608-7622.

85. Korozlu, N., et al., *The elastic and mechanical properties of MB12 (M=Zr, Hf, Y, Lu) as a function of pressure.* Journal of alloys and compounds, 2013. **546**: p. 157-164.

86. Bhat, T.M. and D.C. Gupta, *Effect of on-site Coulomb interaction on electronic and transport properties of 100% spin polarized CoMnVAs.* Journal of Magnetism and Magnetic Materials, 2017. **435**: p. 173-178.

87. Jain, R., et al., *Study of the Electronic Structure, Magnetic and Elastic Properties and Half-Metallic Stability on Variation of Lattice Constants for CoFeCrZ (Z = P, As, Sb) Heusler Alloys.* Journal of superconductivity and novel magnetism, 2017. **31**(8): p. 2399-2409.

88. Srivastava, V., et al., *First-principles study on structural, electronic, magnetic, elastic, mechanical and thermodynamic properties of Mn 2 PtCo Heusler alloy.* International Journal of Energy Research, 2021. **45**(7): p. 11305-11319.

89. Jiang, C., M. Venkatesan, and J.M.D. Coey, *Transport and magnetic properties of Mn2VAl: Search for half-metallicity.* Solid State Communications, 2001. **118**(10): p. 513-516.

90. Chabi, S. and K. Kadel *Two-Dimensional Silicon Carbide: Emerging Direct Band Gap Semiconductor*. Nanomaterials, 2020. **10**, DOI: 10.3390/nano10112226.

91. Wei, X.-P., et al., *Thermoelectric properties of 2D semiconducting Pt2CO2.* Physica Scripta, 2022. **97**(8): p. 085706.

92. Wei, X.-P., et al., *Layer-dependent electronic and magnetic properties for Cr2NO2 and Cr2CO2.* Journal of Magnetism and Magnetic Materials, 2022. **563**: p. 169952.

93. Beth Stearns, M., *Simple explanation of tunneling spin-polarization of Fe, Co, Ni and its alloys.* Journal of Magnetism and Magnetic Materials, 1977. **5**(2): p. 167-171.

94. Rached, H., et al., *A first principle study of phase stability, electronic structure and magnetic properties for Co2−xCrxMnAl Heusler alloys.* Journal of Magnetism and Magnetic Materials, 2015. **379**: p. 84-89.

95. Bourachid, I., et al., *Magneto-electronic and thermoelectric properties of V-based Heusler in ferrimagnetic phase.* Applied Physics A, 2022. **128**(6): p. 1-13.

96. Galanakis, I. and P. H. Dederichs, *Half-Metallicity and Slater-Pauling Behavior in the Ferromagnetic Heusler Alloys*. 2006, Springer Berlin Heidelberg. p. 1-39.

97. Wei, X.-P., P. Gao, and Y.-L. Zhang, *Investigations on Gilbert damping, Curie temperatures and thermoelectric properties in CoFeCrZ quaternary Heusler alloys.* Current Applied Physics, 2020. **20**(4): p. 593-603.

98. Park, S., et al., *Semiclassical Boltzmann transport theory for multi-Weyl semimetals.* Physical Review B, 2017. **95**(16): p. 161113.

99. Hasdeo, E.H., et al., *Optimal band gap for improved thermoelectric performance of two-dimensional Dirac materials.* Journal of Applied Physics, 2019. **126**(3): p. 035109.

100. Slack, G.A., *Nonmetallic crystals with high thermal conductivity.* Journal of Physics and Chemistry of Solids, 1973. **34**(2): p. 321-335.

101. Xiang, H.J. and D.J. Singh, *Suppression of thermopower of ${\mathrm{Na}}_{x}\mathrm{Co}{\mathrm{O}}_{2}$ by an external magnetic field: Boltzmann transport combined with spin-polarized density functional theory.* Physical Review B, 2007. **76**(19): p. 195111.

102. Haleoot, R.E., *Theoretical Investigations of the Electronic, Magnetic, and Thermoelectric Properties of Transition-Metal Based Compounds*. 2019: University of Arkansas.

103. Alqurashi, H., R. Haleoot, and B. Hamad, *First-principles investigations of Zr-based quaternary Heusler alloys for spintronic and thermoelectric applications.* Computational Materials Science, 2022. **210**: p. 111477.

104. Khandy, S.A. and J.-D. Chai, *Thermoelectric properties, phonon, and mechanical stability of new half-metallic quaternary Heusler alloys: FeRhCrZ (Z= Si and Ge).* Journal of Applied Physics, 2020. **127**(16): p. 165102.

105. Alsayegh, S., et al., *First-principal investigations of the electronic, magnetic, and thermoelectric properties of CrTiRhAl quaternary Heusler alloy.* Journal of Magnetism and Magnetic Materials, 2023. **568**: p. 170421.

Appendix

Appendix A: Description of Research for Popular Publication

The insatiable worldwide search for more reliable and secure energy sources has resulted in a significant surge in social and political instability. Many countries are stepping up their R&D efforts in order to provide a more sustainable energy choice. There are a global climate change happening caused using fossil fuels, and that is becoming more serious and need such measures. Hate waste (thermal energy from) the combustion of fossil fuels accounts for over 90% of global electricity production. The typical efficiency of a production facility is between 30 and 40 percent, meaning that 15 terawatts of energy is lost as heat. Thermoelectric generators can recycle waste heat into useable electricity. The amount of heat produced by many industrial and household processes, as well as automotive exhaust, might be turned to energy utilizing thermoelectric devices. Thermoelectric generators are one example of a sustainable and eco-friendly energy source. These devices can convert heat to energy without releasing any greenhouse gases. Since there are no fluids or moving components, these solid-state devices operate quietly. The thermoelectric generator utilizes two kinds of semiconductors, linked thermally in parallel and electrically in series. All naturally occurring substances may be classified as thermoelectric, however, their efficacy varies greatly . That lead to the huge need for investigating thermoelectric materials and finding ways to improve their potential efficiency.

In this study, simulation codes were utilized to identify promising materials for heat-to-electricity conversion. This research aims to find novel thermoelectric materials that have ideal structural, electrical, magnetic, and thermoelectric capabilities for use in spintronic and thermoelectric devices. The simulation is a great tool to investigate thermoelectric material

selection ahead of the time-consuming and costly laboratory experimentation. Novel characteristics, such as high thermoelectric efficiency and half-metallic behavior, are seen in the materials known as Heusler compounds. When a material is half-metallic, it acts as a filter for electrons, allowing only one spin direction (spin-up or spin-down) to pass through. The focus of the study is to present a novel combination of QHA, CrTiRhAl since there are fewer studies investigating Cr-based Heusler compounds. Because of their high melting point and chemical stability at elevated temperatures, QHA Cr-based materials are expected to be particularly promising thermoelectric materials at high temperatures.

Appendix B: Executive Summary of Newly Created Intellectual Property

This research works newly created intellectual property should be taken into account:

1. Thermoelectric properties of CrTiRhAl quaternary Heusler compound.
2. The studied compound transfers into a metallic nonmagnetic material after the Curie temperature.

Appendix C: Potential Patent and Commercialization Aspects of Listed Intellectual Property Items

C.1 Patentability of Intellectual Property (Could Each Item be Patented)

Density functional theory was used to investigate the thermoelectric characteristics of the quaternary Heusler alloy CrTiRhAl QHA. These results could not be patented.

C.2 Commercialization Prospects (Should Each Item Be Patented)

N/A

C.3 Possible Prior Disclosure of IP

1. The results of the work have been published in a journal (see Appendix G).

Appendix D: Broader Impact of Research

D.1 Applicability of Research Methods to Other Problems

The results of investigation CrTiRhAl quaternary Heusler alloy can be utilized to convert heat energy into electricity in thermoelectric devices. Moreover, this quaternary Heusler alloy exhibited 100% spin-polarization and half-metallic behavior, making it a potential material for spintronic applications, spin injectors, spin-valve applications, and magnetic tunnel junctions.

D.2 Impact of Research Results on U.S. and Global Society

The outcomes of this thesis are introducing advance alternative energy sources such as thermoelectric and spintronic devices. Two different semiconductor materials might be used to create thermoelectric devices that convert thermal energy to power energy.

D.3 Impact of research results on the environment

Pollution is one of the downsides of using fossil fuels as the major source of energy. As a result, experts all around the globe are looking for other sources of energy to help lessen this dependency. The goal of this research is to create novel materials with superior magnetic and thermoelectric characteristics for spintronic and thermoelectric applications. These applications are environmentally friendly since they do not produce harmful gases or liquids.

Appendix E: Microsoft Project for MS Micro-EP Degree Plan

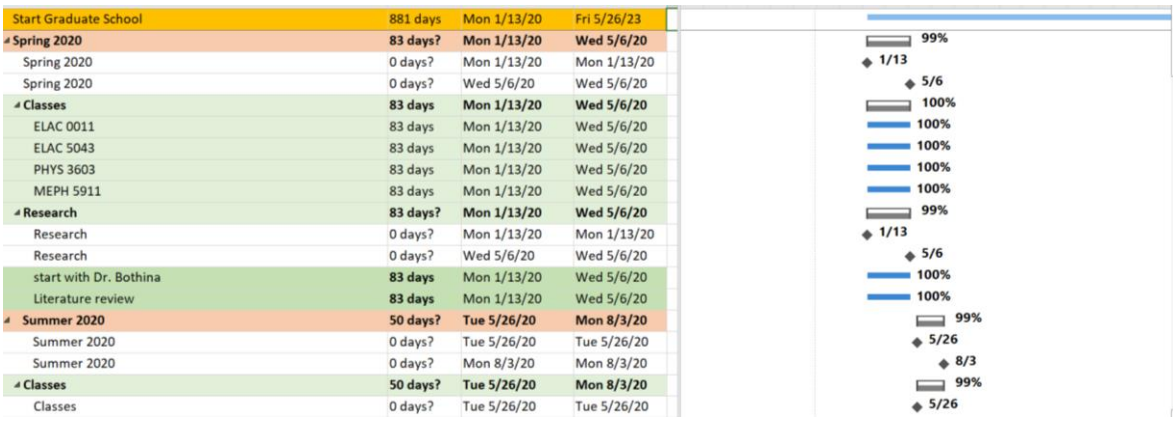

Start Graduate School	881 days	Mon 1/13/20	Fri 5/26/23
Spring 2020	**83 days?**	**Mon 1/13/20**	**Wed 5/6/20**
Spring 2020	0 days?	Mon 1/13/20	Mon 1/13/20
Spring 2020	0 days?	Wed 5/6/20	Wed 5/6/20
Classes	**83 days**	**Mon 1/13/20**	**Wed 5/6/20**
ELAC 0011	83 days	Mon 1/13/20	Wed 5/6/20
ELAC 5043	83 days	Mon 1/13/20	Wed 5/6/20
PHYS 3603	83 days	Mon 1/13/20	Wed 5/6/20
MEPH 5911	83 days	Mon 1/13/20	Wed 5/6/20
Research	**83 days?**	**Mon 1/13/20**	**Wed 5/6/20**
Research	0 days?	Mon 1/13/20	Mon 1/13/20
Research	0 days?	Wed 5/6/20	Wed 5/6/20
start with Dr. Bothina	**83 days**	Mon 1/13/20	Wed 5/6/20
Literature review	**83 days**	Mon 1/13/20	Wed 5/6/20
Summer 2020	**50 days?**	**Tue 5/26/20**	**Mon 8/3/20**
Summer 2020	0 days?	Tue 5/26/20	Tue 5/26/20
Summer 2020	0 days?	Mon 8/3/20	Mon 8/3/20
Classes	**50 days?**	**Tue 5/26/20**	**Mon 8/3/20**
Classes	0 days?	Tue 5/26/20	Tue 5/26/20

MEPH 5821	50 days	Tue 5/26/20	Mon 8/3/20
MATH 2584	50 days	Tue 5/26/20	Mon 8/3/20
Research	**50 days?**	**Tue 5/26/20**	**Mon 8/3/20**
Research	0 days?	Tue 5/26/20	Tue 5/26/20
Research	0 days?	Mon 8/3/20	Mon 8/3/20
Training (LINUX)	50 days	Tue 5/26/20	Mon 8/3/20
Defining my project	50 days	Tue 5/26/20	Mon 8/3/20
Fall 2020	**79 days?**	**Mon 8/24/20**	**Thu 12/10/20**
Fall 2020	0 days?	Mon 8/24/20	Mon 8/24/20
Fall 2020	0 days?	Thu 12/10/20	Thu 12/10/20
Classes	**79 days?**	**Mon 8/24/20**	**Thu 12/10/20**
Classes	0 days?	Mon 8/24/20	Mon 8/24/20
Classes	0 days?	Thu 12/10/20	Thu 12/10/20
MSEN 6811	78 days	Mon 8/24/20	Wed 12/9/20
ELEG 5203	78 days	Mon 8/24/20	Wed 12/9/20
ELEG 3903	77 days	Mon 8/24/20	Tue 12/8/20
Research	**79 days?**	**Mon 8/24/20**	**Thu 12/10/20**
Research	0 days?	Mon 8/24/20	Mon 8/24/20
Research	0 days?	Thu 12/10/20	Thu 12/10/20

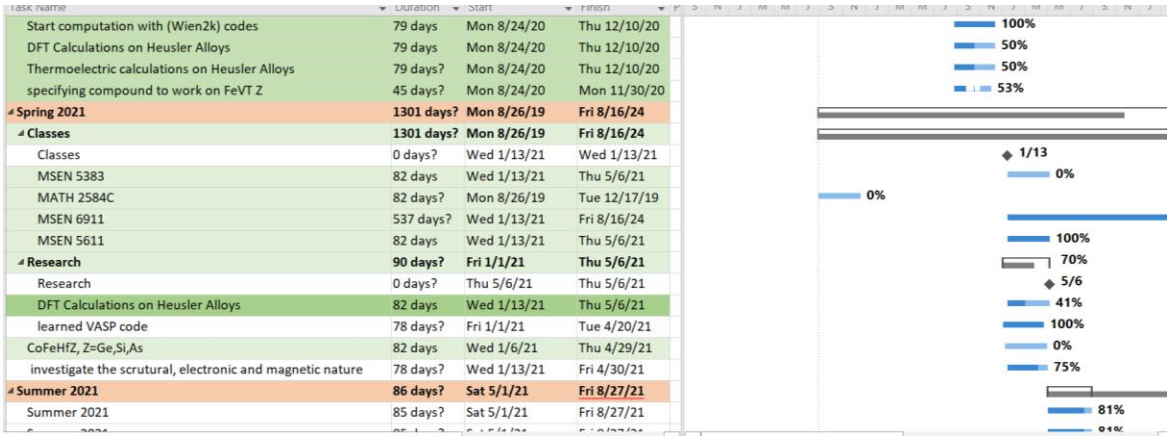

Task Name	Duration	Start	Finish
Start computation with (Wien2k) codes	79 days	Mon 8/24/20	Thu 12/10/20
DFT Calculations on Heusler Alloys	79 days	Mon 8/24/20	Thu 12/10/20
Thermoelectric calculations on Heusler Alloys	79 days?	Mon 8/24/20	Thu 12/10/20
specifying compound to work on FeVT Z	45 days?	Mon 8/24/20	Mon 11/30/20
Spring 2021	**1301 days?**	**Mon 8/26/19**	**Fri 8/16/24**
Classes	**1301 days?**	**Mon 8/26/19**	**Fri 8/16/24**
Classes	0 days?	Wed 1/13/21	Wed 1/13/21
MSEN 5383	82 days	Wed 1/13/21	Thu 5/6/21
MATH 2584C	82 days?	Mon 8/26/19	Tue 12/17/19
MSEN 6911	537 days?	Wed 1/13/21	Fri 8/16/24
MSEN 5611	82 days	Wed 1/13/21	Thu 5/6/21
Research	**90 days?**	**Fri 1/1/21**	**Thu 5/6/21**
Research	0 days?	Thu 5/6/21	Thu 5/6/21
DFT Calculations on Heusler Alloys	82 days	Wed 1/13/21	Thu 5/6/21
learned VASP code	78 days?	Fri 1/1/21	Tue 4/20/21
CoFeHfZ, Z=Ge,Si,As	82 days	Wed 1/6/21	Thu 4/29/21
investigate the scrutural, electronic and magnetic nature	78 days?	Wed 1/13/21	Fri 4/30/21
Summer 2021	**86 days?**	**Sat 5/1/21**	**Fri 8/27/21**
Summer 2021	85 days?	Sat 5/1/21	Fri 8/27/21

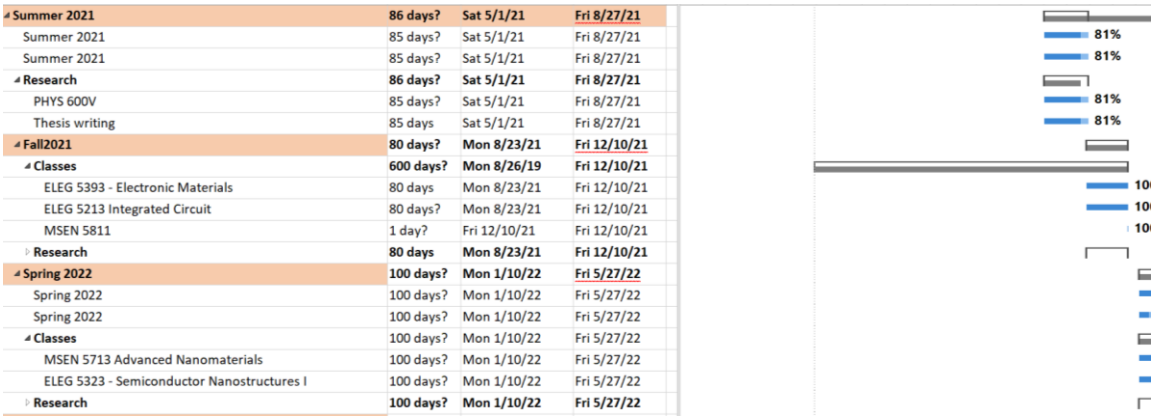

Summer 2021	**86 days?**	**Sat 5/1/21**	**Fri 8/27/21**
Summer 2021	85 days?	Sat 5/1/21	Fri 8/27/21
Summer 2021	85 days?	Sat 5/1/21	Fri 8/27/21
Research	**86 days?**	**Sat 5/1/21**	**Fri 8/27/21**
PHYS 600V	85 days?	Sat 5/1/21	Fri 8/27/21
Thesis writing	85 days	Sat 5/1/21	Fri 8/27/21
Fall2021	**80 days?**	**Mon 8/23/21**	**Fri 12/10/21**
Classes	**600 days?**	**Mon 8/26/19**	**Fri 12/10/21**
ELEG 5393 - Electronic Materials	80 days	Mon 8/23/21	Fri 12/10/21
ELEG 5213 Integrated Circuit	80 days?	Mon 8/23/21	Fri 12/10/21
MSEN 5811	1 day?	Fri 12/10/21	Fri 12/10/21
Research	**80 days**	**Mon 8/23/21**	**Fri 12/10/21**
Spring 2022	**100 days?**	**Mon 1/10/22**	**Fri 5/27/22**
Spring 2022	100 days?	Mon 1/10/22	Fri 5/27/22
Spring 2022	100 days?	Mon 1/10/22	Fri 5/27/22
Classes	100 days?	Mon 1/10/22	Fri 5/27/22
MSEN 5713 Advanced Nanomaterials	100 days?	Mon 1/10/22	Fri 5/27/22
ELEG 5323 - Semiconductor Nanostructures I	100 days?	Mon 1/10/22	Fri 5/27/22
Research	**100 days?**	**Mon 1/10/22**	**Fri 5/27/22**

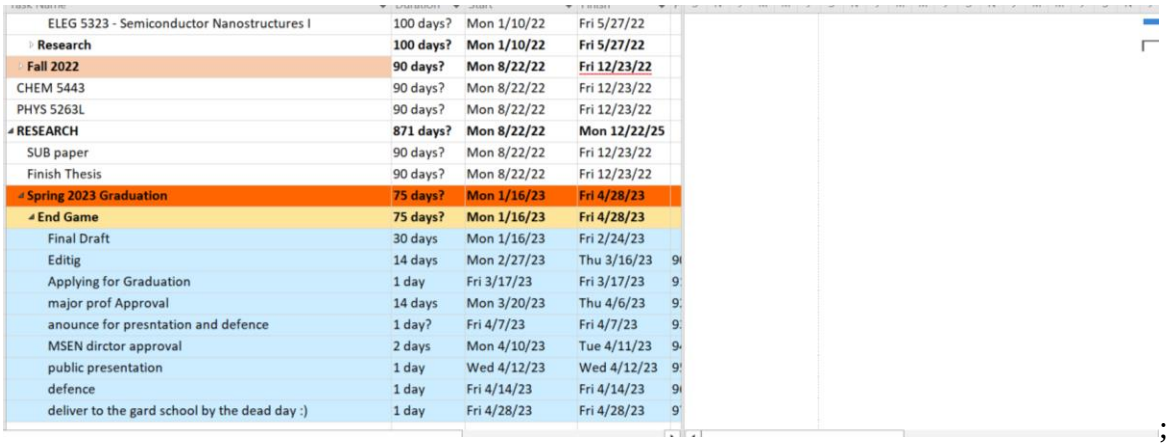

ELEG 5323 - Semiconductor Nanostructures I	100 days?	Mon 1/10/22	Fri 5/27/22
Research	**100 days?**	**Mon 1/10/22**	**Fri 5/27/22**
Fall 2022	**90 days?**	**Mon 8/22/22**	**Fri 12/23/22**
CHEM 5443	90 days?	Mon 8/22/22	Fri 12/23/22
PHYS 5263L	90 days?	Mon 8/22/22	Fri 12/23/22
RESEARCH	**871 days?**	**Mon 8/22/22**	**Mon 12/22/25**
SUB paper	90 days?	Mon 8/22/22	Fri 12/23/22
Finish Thesis	90 days?	Mon 8/22/22	Fri 12/23/22
Spring 2023 Graduation	**75 days?**	**Mon 1/16/23**	**Fri 4/28/23**
End Game	**75 days?**	**Mon 1/16/23**	**Fri 4/28/23**
Final Draft	30 days	Mon 1/16/23	Fri 2/24/23
Editig	14 days	Mon 2/27/23	Thu 3/16/23
Applying for Graduation	1 day	Fri 3/17/23	Fri 3/17/23
major prof Approval	14 days	Mon 3/20/23	Thu 4/6/23
anounce for presntation and defence	1 day?	Fri 4/7/23	Fri 4/7/23
MSEN dirctor approval	2 days	Mon 4/10/23	Tue 4/11/23
public presentation	1 day	Wed 4/12/23	Wed 4/12/23
defence	1 day	Fri 4/14/23	Fri 4/14/23
deliver to the gard school by the dead day :)	1 day	Fri 4/28/23	Fri 4/28/23

;

Appendix F: Identification of all software used in research and thesis generation

Computer #1: Personal Laptop

Device ID: 2CAE9544-E487-457E-85F4-69A1F92D3113

Product ID: 00342-20757-35086-AAOEM

Owner: Shuruq Alsayegh

Computer #2: Personal Laptop

Model Number: N/A

Owner: Shuruq Alsayegh

Software #1: Name: Ubuntu

license: downloaded by Shuruq Alsayegh

Software #2: Name: XMGRACE

license: downloaded by Shuruq Alsayegh

Software #3:

Name: VESTA

Free license: downloaded by Shuruq Alsayegh

Software #4:

Name: Endnote

Free license: downloaded by Shuruq Alsayegh

Software #5:

Name: Adobe Illustrator

Purchased by: Shuruq Alsayegh

Software #6:

Name: Microsoft Word

Appendix G: All publications published, submitted, and planned Publications

Chapter 4 was originally published as [105]:

Alsayegh S, Alqurashi H, Andharih E, Hamad B, Manasreh MO. First-principal investigations of the electronic, magnetic, and thermoelectric properties of CrTiRhAl quaternary Heusler alloy. Journal of Magnetism and Magnetic Materials 2023;568:170421.